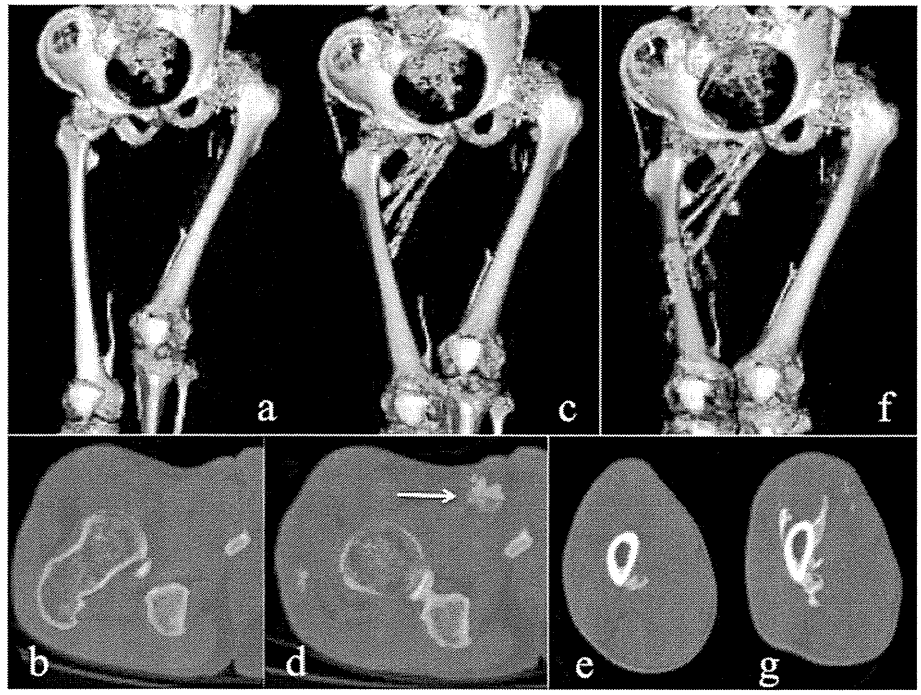

Figure 3 CT images from Case 2. Reconstructed 3D-CT images of the pelvis and bilateral femora at baseline **(a)**, at M-12 m **(c)**, and at D-12 m **(f)**. Axial CT images of the right hip at baseline **(b)**, and at M-12 m **(d)**, and those of the right mid-femur at M-12 m **(e)**, and at D-12 m **(g)**. Heterotopic ossifications in the right adductor muscle (arrow) developed during the medication phase and around mid-femur developed during the discontinuation phase ware clearly demonstrated.

bone volume of 536 cm^3 during the discontinuation phase, which appeared to reflect maturation of the iliopsoas ossification and newly developed bones in the gluteus medius (Figure 4e-g) and around the right jaw joints (Figure 4h,i).

Discussion

To date, there are few clinical trials in the treatment of FOP. Zasloff et al. [14] conducted a prospective study to assess the efficacy of isotretinoin (13-cis-retinoic acid) in the prevention of heterotopic ossification in FOP, and concluded that isotretinoin had no apparent effect in the prevention of new bone formation after surgery or after soft tissue trauma. Brantus and Meunier [15] evaluated the effects of intravenous administration of etidronate and oral corticosteroids for thirty-one FOP attacks in seven patients, and observed 10 new ossifications causing severe deterioration of joint mobility during the mean six years of follow up. These studies indicated that there is no proven efficacy with any therapy in changing the natural history of the disease. Despite the Pex treatment, heterotopic ossification developed rapidly in our two patients suggesting that oral administration of Pex within 0.15-0.60 mg/L seemed to be unsatisfactory in the inhibition of heterotopic ossifications in FOP. Moreover, there is a concerning possibility that Pex administration unexpectedly induced heterotopic ossification in these patients.

Abnormal biochemical measurements of bone mineral metabolism have rarely been reported in FOP [16]. Establishment of useful biomarkers as correlates of disease severity and clinical outcome is desirable to enable early proof-of-concept studies that can help screen potential drug candidates and identify therapeutic targets. Kaplan et al. [17] described that serum ALP activity may increase during disease flare-ups. Our serial clinical and biochemical evaluations demonstrated that elevation of serum ALP and BAP, which synchronized with acute flare-ups, preceded the heterotopic new bone formations. Serum levels of ALP or BAP could be useful biomarkers for monitoring the development of heterotopic ossifications and efficacy of the therapy in FOP.

Multi-detector-row CT has widely been used in clinical environments, and whole body scanning allows 3D structural characterization of entire bone segment at high resolution [18]. Despite the restricted movement and joint immobilization of our patients, standardization of ROI in each individual could allow for accurate volume calculating capabilities. To the best of our

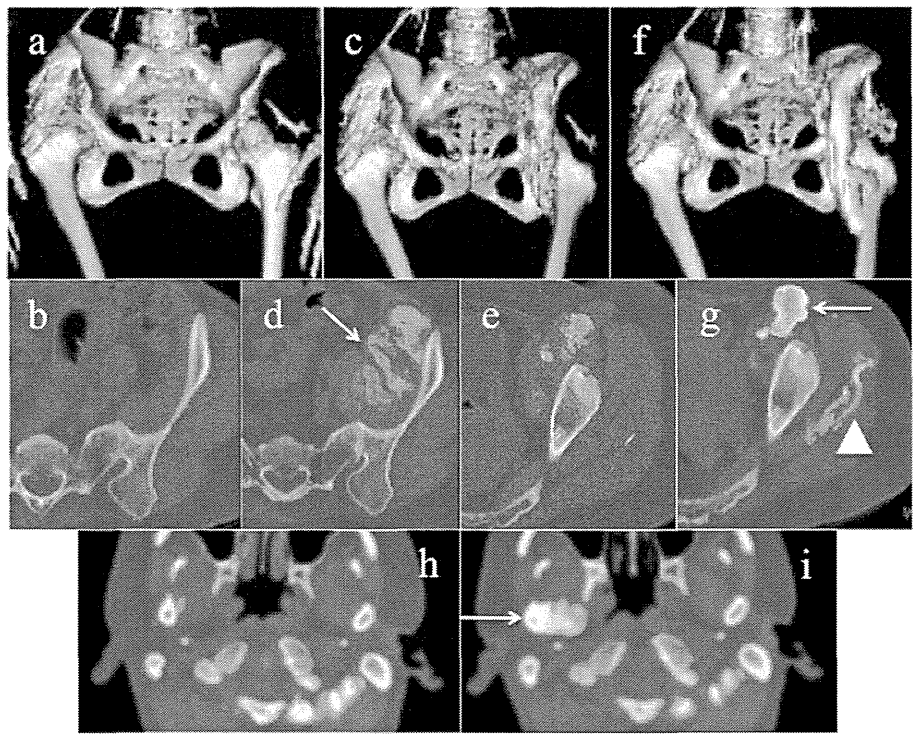

Figure 4 CT images form Case 3. Reconstructed 3D-CT images of the hip joints at baseline **(a)**, at M-12 m **(c)**, and at D-12 m **(f)**. Axial CT images of the left pelvis at baseline **(b)**, at M-12 m **(d, e)**, and at D-12 m **(g)**, and those of the bilateral jaws at M-12 m **(h)**, and at D-12 m **(i)**. Massive new bone formations in the left iliac muscle were developed during the medication phase **(d**, arrow**)**. During the discontinuation phase, the left intra-iliopsoas ossification matured **(g**, arrow**)**, and heterotopic boned in the left gluteus medius **(g**, arrow head**)** and the right jaw joint **(i**, arrow**)** were newly formed.

knowledge, no studies have presented quantitative assessment of ectopic bone formations in FOP. Volumetric 3D-CT analyses demonstrated that change in the total bone volume correlated with the clinical symptoms and laboratory examinations in two patients who showed active flare-ups. Our study highlights greater capabilities of whole body CT scanning as an evaluation tool for disease progression in FOP, especially in assessment of treatment efficacy during forthcoming clinical trials.

There are several major limitations in the present study. First, since there are no better natural history studies for FOP to date, it is difficult to design any clinical trial with meaningful endpoints. Furthermore, we do not know the natural evolution of ectopic bone formations in our patients. Second, the present study could not be designed for pediatric FOP patients because of uncertainty in safety, tolerability, and pharmacokinetics of Pex in the pediatric population. Third, heterotopic ossification in FOP is generally formed via an endochondral ossification process, but we did not confirm heterotopic cartilage formation in our patients. Quantification of total bone volume based on 3D-CT images could be a reliable evaluation tool for assessment of ectopic bone formations, but radiation exposure by CT examination may be a major issue for young patients. Besides, whole body scanning has always been uncomfortable for severely deformed FOP patients, although it takes less than five minutes. Without scanning the whole body, heterotopic ossification following flare-ups (if they occur) could be evaluated by a narrow scan around the flare-ups region. For future clinical trials, standardization of imaging protocol will be expected in evaluating heterotopic bones in FOP.

Conclusions

Although the number of patients is too small to draw reliable conclusions, oral administration of Pex within the safety dose seemed not to be effective in the inhibition of heterotopic ossifications in FOP, despite the absence of significant adverse effects.

Abbreviations

FOP: Fibrodysplasia ossificans progressiva; ACVR1: Activin A receptor type I; ALK2: Activin-like kinase 2; BMP: Bone morphogenetic protein; Pex: Perhexiline maleate; NSAIDs: Nonsteroidal anti-inflammatory drugs; COX-2: Cyclooxygenase-2; CT: Computed tomography; ALP: Alkaline phosphatase; BAP: Bone-specific alkaline phosphatase; OC: Osteocalcin; JSCC: Japan society of clinical chemistry; EIA: Enzyme immunoassay; RIA: Radioimmunoassay;

3D: Three-dimensional; ROI: Regions of interest; IFOPA: International Fibrodysplasia ossificans progressiva association.

Competing interests
The authors declare that they have no competing interests.

Authors' contribution
H Kitoh did most of the patients' follow up, participated in the whole study and drafted the manuscript. MA did the CT interpretations. H Kaneko, MK, MM, IK participated in the clinical trial. JDH and BCS measured plasma concentration of Pex and suggested an optimal dose of Pex administration. KO and NI participated in the design of the study. All authors contributed to elaborating the manuscript. All authors read and approved the final manuscript.

Authors' information
H Kitoh is a member of the Japanese Research Committee on Fibrodysplasia Ossificans Progressiva.

Acknowledgements
This work was supported in partly by Research Committee on Fibrodysplasia Ossificans Progressiva form the Ministry of Health, Labour and Welfare of Japan.

Author details
[1]Department of Orthopaedic Surgery, Nagoya University Graduate School of Medicine, 65 Tsurumai, Showa-ku, Nagoya, Aichi 466-8550, Japan. [2]Department of Radiological Technology, Nagoya University Graduate School of Medicine, 65 Tsurumai, Showa-ku, Nagoya, Aichi 466-8550, Japan. [3]Department of Rehabilitation, Nagoya University Graduate School of Medicine, 65 Tsurumai, Showa-ku, Nagoya, Aichi 466-8550, Japan. [4]Department of Cardiology and Clinical Pharmacology, Queen Elizabeth Hospital, 28 Woodville Road, Woodville, SA 5011, Australia. [5]Division of Neurogenetics, Center for Neurological Diseases and Cancer, Nagoya University Graduate School of Medicine, 65 Tsurumai, Showa-ku, Nagoya, Aichi 466-8550, Japan.

Received: 24 April 2013 Accepted: 13 October 2013
Published: 16 October 2013

References
1. Shore EM, Feldman GJ, Xu M, Kaplan FS: **The genetics of fibrodysplasia ossificans progressiva.** *Clin Rev Bone Miner Metab* 2005, **3**:201–204.
2. Shore EM, Xu M, Feldman GJ, Fenstermacher DA, Cho T-J, Choi IH, Connor JM, Delai P, Glaser DL, Le Merrer M, Morhart R, Rogers JG, Smith R, Triffitt JT, Urtizberea JA, Zasloff M, Brown MA, Kaplan FS: **A recurrent mutation in the BMP type I receptor ACVR1 causes inherited and sporadic fibrodysplasia ossificans progressiva.** *Nat Genet* 2006, **38**:525–527.
3. Kaplan FS, Chakkalakal SA, Shore EM: **Fibrodysplasia ossificans progressiva: mechanisms and models of skeletal metamorphosis.** *Dis Model Mech* 2012, **5**:756–762.
4. Pignolo RJ, Shore EM, Kaplan FS: **Fibrodysplasia ossificans progressiva: Clinical and genetic aspects.** *Orphanet J Rare Dis* 2011, **6**:80.
5. Cohen RB, Hahn GV, Tabas JA, Peeper J, Levitz CL, Sando A, Sando N, Zasloff M, Kaplan FS: **The natural history of heterotopic ossification in patients who have fibrodysplasia ossificans progressiva. A study of forty-four patients.** *J Bone Joint Surg Am* 1993, **75**:215–219.
6. Yu PB, Hong CC, Sachidanandan C, Babitt JL, Deng DY, Hoyng SA, Lin HY, Bloch KD, Peterson RT: **Dorsomorphin inhibits BMP signals required for embryogenesis and iron metabolism.** *Nat Chem Biol* 2008, **4**:33–441.
7. Yu PB, Deng DY, Lai CS, Hong CC, Cuny GD, Bouxsein ML, Hong DW, McManus PM, Katagiri T, Sachidanandan C, *et al*: **BMP type I receptor inhibition reduces heterotopic [corrected] ossification.** *Nat Med* 2008, **14**:1363–1369.
8. Shimono K, Tung WE, Macolino C, Chi AH, Didizian JH, Mundy C, Chandraratna RA, Mishina Y, Enomoto-Iwamoto M, Pacifici M, Iwamoto M: **Potent inhibition of heterotopic ossification by nuclear retinoic acid receptor-gamma agonists.** *Nat Med* 2011, **17**:454–460.
9. Abbott A: **Neurologists strike gold in drug screen effort.** *Nature* 2002, **417**:109.
10. Yamamoto R, Matsushita M, Kitoh H, Masuda A, Ito M, Katagiri T, Kawai T, Ishiguro N, Ohno K: **Clinically applicable antianginal agents suppress osteoblastic transformation of myogenic cells and heterotopic ossifications in mice.** *J Bone Miner Metab* 2013, **31**:26–33.
11. Fukuda T, Kohda M, Kanomata K, Nojima J, Nakamura A, Kamizono J, Noguchi Y, Iwakiri K, Kondo T, Kurose J, Endo K, Awakura T, Fukushi J, Nakashima Y, Chiyonobu T, Kawara A, Nishida Y, Wada I, Akita M, Komori T, Nakayama K, Nanba A, Maruki Y, Yoda T, Tomoda H, Yu PB, Shore EM, Kaplan FS, Miyazomo K, Matsuoka M, *et al*: **Constitutively activated ALK2 and increases SMAD1/5 cooperatively induce bone morphogenetic protein signaling in fibrodysplasia ossificans progressiva.** *J Biol Chem* 2009, **284**:7149–7156.
12. Shah RR, Oates NS, Idle JR, Smith RL, Lockhart JD: **Impaired oxidation of debrisoquine in patients with perhexiline neuropathy.** *Br Med J* 1982, **284**:295–299.
13. *International Fibrodysplasia Ossificans Progressiva Association.* [http://www.ifopa.org/en/living-with-fop-menu/treatment-guidelines.html]
14. Zasloff MA, Roche DM, Crofford LJ, Hahn GV, Kaplan FS: **Treatment of patients who have fibrodysplasia ossificans progressiva with isotretinoin.** *Clin Orthop* 1998, **346**:121–129.
15. Brantus JF, Meunier PJ: **Effects of intravenous etidronate and oral corticosteroids in fibrodysplasia ossificans progressiva.** *Clin Orthop* 1998, **346**:117–120.
16. Blumenkrantz N, Asboe-Hansen G: **Fibrodysplasia ossificans progressiva. Biochemical changes in blood serum, urine, skin, bone, and ectopic ossification.** *Scand J Rheumatol* 1978, **7**:85–89.
17. Kaplan FS, LeMerrer M, Glaser DL, Pignolo RJ, Goldsby RE, Kitterman JA, Groppe J, Shore EM: **Fibrodysplasia ossificans progressiva.** *Best Pract Res Clin Rheumatol* 2008, **22**:191–205.
18. Ptak T, Rhea JT, Novelline RA: **Radiation dose is reduced with a single-pass whole-body multi-detector row CT trauma protocol compared with a conventional segmented method: initial experience.** *Radiology* 2003, **229**:902–905.

doi:10.1186/1750-1172-8-163
Cite this article as: Kitoh *et al.*: Perhexiline maleate in the treatment of fibrodysplasia ossificans progressiva: an open-labeled clinical trial. *Orphanet Journal of Rare Diseases* 2013 **8**:163.

OPEN ACCESS Freely available online

PLOS ONE

Meclozine Facilitates Proliferation and Differentiation of Chondrocytes by Attenuating Abnormally Activated FGFR3 Signaling in Achondroplasia

Masaki Matsushita[1,2], Hiroshi Kitoh[2], Bisei Ohkawara[1], Kenichi Mishima[1,2], Hiroshi Kaneko[1,2], Mikako Ito[1], Akio Masuda[1], Naoki Ishiguro[2], Kinji Ohno[1]*

1 Division of Neurogenetics, Center for Neurological Diseases and Cancer, Nagoya University Graduate School of Medicine, Nagoya, Japan, **2** Department of Orthopaedic Surgery, Nagoya University Graduate School of Medicine, Nagoya, Japan

Abstract

Achondroplasia (ACH) is one of the most common skeletal dysplasias with short stature caused by gain-of-function mutations in FGFR3 encoding the fibroblast growth factor receptor 3. We used the drug repositioning strategy to identify an FDA-approved drug that suppresses abnormally activated FGFR3 signaling in ACH. We found that meclozine, an anti-histamine drug that has long been used for motion sickness, facilitates chondrocyte proliferation and mitigates loss of extracellular matrix in FGF2-treated rat chondrosarcoma (RCS) cells. Meclozine also ameliorated abnormally suppressed proliferation of human chondrosarcoma (HCS-2/8) cells that were infected with lentivirus expressing constitutively active mutants of FGFR3-K650E causing thanatophoric dysplasia, FGFR3-K650M causing SADDAN, and FGFR3-G380R causing ACH. Similarly, meclozine alleviated abnormally suppressed differentiation of ATDC5 chondrogenic cells expressing FGFR3-K650E and -G380R in micromass culture. We also confirmed that meclozine alleviates FGF2-mediated longitudinal growth inhibition of embryonic tibia in bone explant culture. Interestingly, meclozine enhanced growth of embryonic tibia in explant culture even in the absence of FGF2 treatment. Analyses of intracellular FGFR3 signaling disclosed that meclozine downregulates phosphorylation of ERK but not of MEK in FGF2-treated RCS cells. Similarly, meclozine enhanced proliferation of RCS cells expressing constitutively active mutants of MEK and RAF but not of ERK, which suggests that meclozine downregulates the FGFR3 signaling by possibly attenuating ERK phosphorylation. We used the C-natriuretic peptide (CNP) as a potent inhibitor of the FGFR3 signaling throughout our experiments, and found that meclozine was as efficient as CNP in attenuating the abnormal FGFR3 signaling. We propose that meclozine is a potential therapeutic agent for treating ACH and other FGFR3-related skeletal dysplasias.

Citation: Matsushita M, Kitoh H, Ohkawara B, Mishima K, Kaneko H, et al. (2013) Meclozine Facilitates Proliferation and Differentiation of Chondrocytes by Attenuating Abnormally Activated FGFR3 Signaling in Achondroplasia. PLoS ONE 8(12): e81569. doi:10.1371/journal.pone.0081569

Editor: Oreste Gualillo, SERGAS, Santiago University Clinical Hospital, IDIS Research Laboratory 9, NEIRID Lab, Spain

Received April 12, 2013; **Accepted** October 15, 2013; **Published** December 4, 2013

Funding: This work was supported by Grants-in-Aid from the Ministry of Education, Culture, Sports, Science, and Technology of Japan, and the Ministry of Health, Labor, and Welfare of Japan. The funders had no role in study design, data collection and analysis, decision to publish, or preparation of the manuscript.

Competing Interests: The authors have declared that no competing interests exist.

* E-mail: ohnok@med.nagoya-u.ac.jp

Introduction

Achondroplasia (ACH) is one of the most common skeletal dysplasias with an incidence of one in 16,000 to 26,000 live births [1]. Clinical features of ACH include rhizomelic short stature, apparent macrocephaly with midface hypoplasia, bowing of the lower limbs, and increased lumbar lordosis [2]. ACH is caused by gain-of-function mutations in the fibroblast growth factor receptor 3 (*FGFR3*) gene [3,4]. FGFR3 is a key regulator of endochondral bone growth, which signals through several intracellular pathways including the signal transducer and activator of transcription (STAT) and mitogen-activated protein kinase (MAPK) [5–7]. Gain-of-function mutations of *FGFR3* cause several short-limbed skeletal dysplasias such as hypochondroplasia (HCH) [8], severe ACH with developmental delay and acanthosis nigricans (SADDAN) [9], and thanatophoric dysplasia (TD) types I and II [10]. In contrast, loss of function mutations in *FGFR3* lead to the CATSHL syndrome in humans, which is characterized by overgrowth of the skeleton including camptodactyly, tall stature, scoliosis, and hearing loss [11], as well as spider lamb syndrome in sheep [12]. These findings indicate that the FGFR3 signaling functions as a negative regulator of endochondral bone growth.

No effective treatments for FGFR3-related skeletal dysplasias are currently available. Growth hormone (GH) has been administered to children with ACH based on evidence of a short-term beneficial effect [13]. The response to GH, however, is moderate and the long-term effect remains controversial. It is conceivable that downregulation of the FGFR3 signaling alleviates the skeletal phenotype of FGFR3-related skeletal dysplasias. Small chemical compounds that antagonize the FGFR3 signaling have recently been identified. Toxicological profiles of these compounds, however, remain mostly unresolved [14-16]. The C-type natriuretic peptide (CNP) is a potent antagonist of the FGFR3 signaling that alleviates the short-limbed phenotype of ACH mice through its inhibition of the FGFR3-MAPK pathway [6,17]. CNP has a short half-life and continuous intravenous infusion is required for *in vivo* experiments [18]. The CNP analog with an extended half-life, BMN 111, has recently been developed and

significant recovery of bone growth was demonstrated in ACH mice by subcutaneous administration of BMN 111 [19].

The drug repositioning strategy, in which a drug currently used for patients with a specific disease is applied to another disease, has gained increasing attention from both academia and industry in recent years [20,21]. The advantage of this strategy is that the identified drugs can be readily applied to clinical practice, because the optimal doses and adverse effects are already established. Here, we screened 1,186 FDA-approved compounds to identify a clinically applicable drug that ameliorates ACH and other FGFR3-related skeletal dysplasias. We found that meclozine dihydrochloride, a commonly used anti-emetic drug for its anti-histamine activity, efficiently suppresses FGFR3 signaling in three different chondrocytic cell lines and embryonic bone organ culture. We also identified that meclozine suppresses FGF2-mediated phosphorylation of ERK.

Results

Meclozine facilitates chondrocyte proliferation and mitigates loss of extracellular matrix in FGF2-treated RCS cells

As rat chondrosarcoma (RCS) chondrocytic cells express high levels of FGFR3, exogenous administration of FGF2 readily recapitulates cellular processes occurring in FGFR3-related skeletal dysplasias [22]. We thus added 10 μM of 1,186 FDA-approved chemical compounds (Prestwick Chemical) along with 5 ng/ml FGF2 to the RCS cells. Quantification of RCS proliferation by the MTS assay revealed that meclozine consistently induced 1.4-fold or more increases in RCS proliferation. In addition, 0, 1, 2, 5, 10, and 20 μM of meclozine exhibited dose-dependent increases in RCS proliferation (Figure 1A). We did not observe dose-dependency at 50 μM, which was likely due to cell toxicity. We also confirmed that 10 and 20 μM of meclozine increased the number of RCS cells (Figure 1B).

We next compared the effect of meclozine with that of CNP [6,17] as a positive control. Growing RCS cells produced a large amount of cartilage-like sulfated proteoglycans, which were visualized by Alcian blue staining (Figure 1C). The matrix proteoglycans were almost completely lost at 72 hours after addition of FGF2 due to inhibition of proteoglycan production and also to induction of matrix metalloproteinase-mediated degradation [6]. Treatment of FGF2-added RCS cells with meclozine partly restored staining for Alcian blue and round chondrocyte-like cell shapes, which were similar to those observed with CNP.

We first confirmed that treating RCS cells with FGF2 for four hours induced expressions of matrix metalloproteinase 10 (*Mmp10*), *Mmp13*, and a disintegrin-like and metalloproteinase with thrombospondin type 1 motif 1 (*Adamts1*) transcripts, as has been previously reported [6]. We found that meclozine and CNP significantly suppressed expressions of these matrix metalloproteinases (Figure 1D). We also quantified expressions of *Col2a1* and *Acan* transcripts, but FGF2 treatment for 72 hours did not reduce the expression levels of these genes in RCS cells (Figure S1). Meclozine thus decreases expressions of the matrix metalloproteinases in FGF2-treated RCS cells.

Meclozine mitigates abnormally suppressed proliferation of HCS-2/8 chondrocytes expressing FGFR3-K650E, -K650M, and -G380R

We examined the effects of meclozine on chondrocyte proliferation under the influence of FGFR3 mutants. As RCS cells express high levels of wild-type FGFR3, we used human chondrosarcoma (HCS-2/8) cells to observe unequivocal effects of the transduced FGFR3 mutants. We first introduced lentivirus carrying active mutants of FGFR3 (K650E in TDII, K650M in SADDAN, and G380R in ACH) into HCS-2/8 cells. The lentivirus carried IRES2-driven Venus cDNA downstream of FGFR3 cDNA. The MTS assay demonstrated that K650E-expressing HCS-2/8 cells showed significantly suppressed cellular proliferation (Figure S2). Meclozine partially rescued the growth arrest without apparent cellular toxicity in HCS-2/8 cells expressing the three FGFR3 mutants (Figure 2A). We also observed that the areas of Venus signals, which should be proportional to the number of Venus-positive cells, were increased by meclozine as well as by CNP in K650E- and G380R-expressing HCS-2/8 cells (Figure 2B).

Meclozine mitigates abnormally suppressed differentiation of ATDC5 chondrogenic cells expressing FGFR3-G380R and -K650E in micromass culture

We next examined the effects of meclozine on chondrocyte differentiation in the presence of FGFR3 mutants. ATDC5 cells retain potency to differentiate into chondrocytes and are commonly used to study chondrogenesis *in vitro* [15]. We added meclozine to the micromass culture of ATDC5 cells that were infected with lentivirus expressing FGFR3-wild-type, FGFR3-G380R, or -K650E. Alcian blue staining revealed abundant sulfated proteoglycans on wild-type FGFR3 cells, while the staining intensity was reduced by the mutations. Addition of meclozine simultaneously with the chondrogenic induction alleviated the inhibitory effect of the G380R and K650E with and without statistical significance, respectively. Quantitative analysis of sulfated glycosaminoglycans in cell lysate demonstrated that meclozine increased the levels of glycosaminoglycans (Figure 3).

Meclozine increases the longitudinal length of embryonic tibiae with or without FGF2 treatment in bone explant culture

We further quantified the effect of meclozine on FGF2-mediated inhibition of cartilage development in the bone organ culture employing limb rudiments isolated from developing murine embryonic tibia [14]. We added combinations of 100 ng/ml FGF2, 0.2 μM CNP, and 20 μM meclozine to the culture medium, and compared the length of treated tibiae with that of contralateral control tibia from the same individual. The addition of FGF2 inhibited longitudinal growth of bone and cartilage of embryonic tibiae, while CNP and meclozine significantly attenuated the growth inhibition driven by FGF2 (Figure 4). Histological analysis revealed that FGF2 treatment reduced the thickness of the hypertrophic chondrocyte layer, while treatments with CNP and meclozine mitigated the effect of FGF2 (Figure S4). It is interesting to note that meclozine also increased the length of tibia without FGF2 treatment but without statistical significance.

Meclozine attenuates ERK phosphorylation in FGF2-treated RCS cells

We next scrutinized the effects of meclozine on the downstream signaling pathways of FGFR3 in FGF2-treated RCS cells. RCS cells were pretreated with meclozine for 30 minutes before adding FGF2, and the phosphorylation levels of ERK and MEK were determined by Western blotting. The FGF2-mediated ERK1/2 phosphorylation was attenuated by meclozine, while MEK1/2 phosphorylation remained unchanged (Figure 5A). We next introduced constitutively active (ca) mutants of ERK, MEK, and

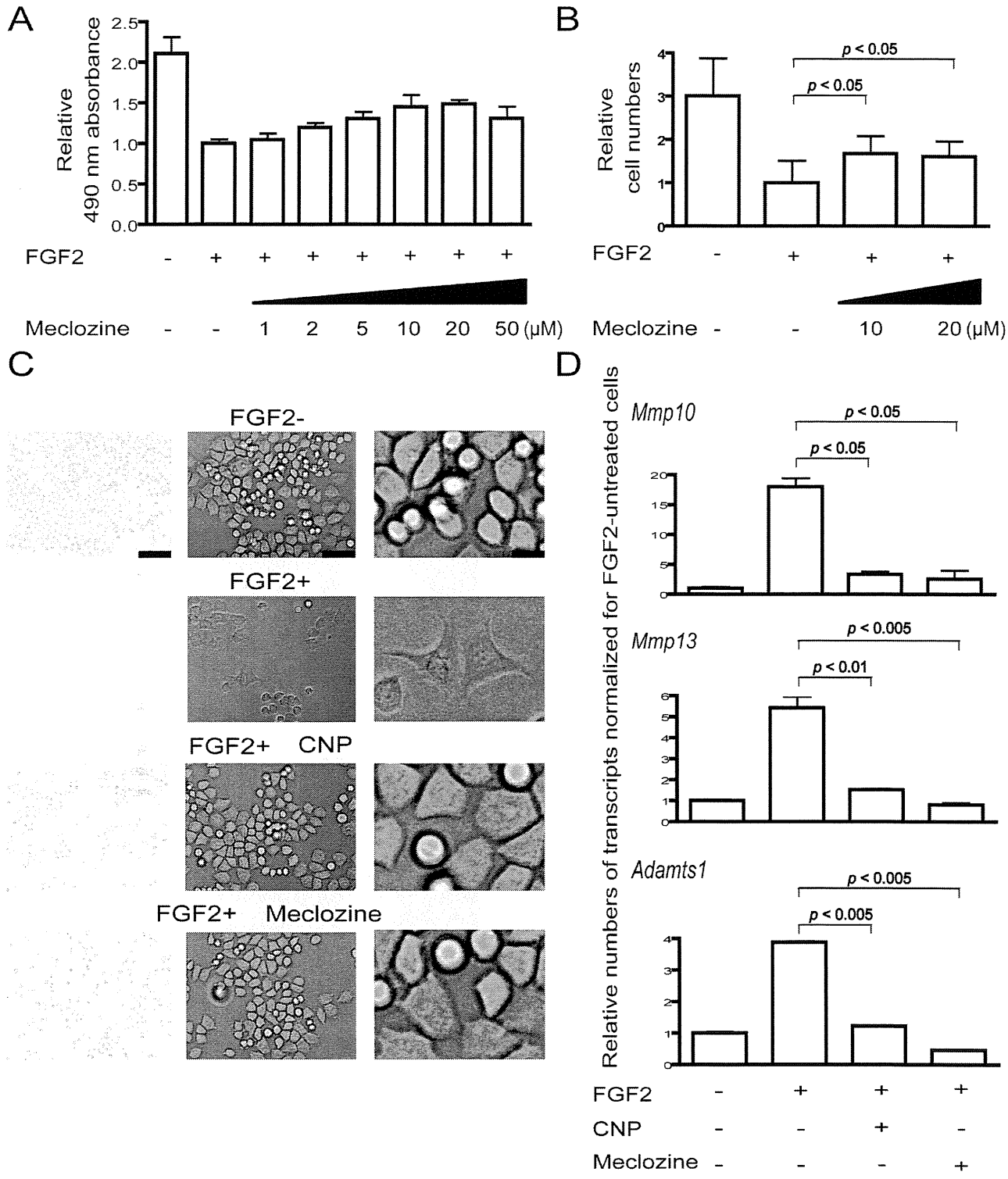

Figure 1. Meclozine promotes chondrocyte proliferation and ameliorates loss of extracellular matrix in FGF2-treated RCS cells. (A, B) RCS cells were treated with 5 ng/ml FGF2 and the indicated concentrations of meclozine for 48 hours. Cell growth was quantified using the MTS assay (A) or by counting cells (B). Data are normalized to that without meclozine and indicated by the mean and SD ($n = 8$ for A and 6 for B). Meclozine rescued the FGF2-mediated growth arrest of RCS cells. (C) Meclozine (10 μM) ameliorated FGF2-mediated alteration of cellular shape and loss of extracellular matrix. RCS cells were treated with 5 ng/ml FGF2 with and without 0.2 μM CNP or 20 μM meclozine for 72 hours, and cartilage-like sulfated proteoglycan matrix was stained by Alcian blue. Growing RCS cells were round-shaped and produced abundant cartilage-like sulfated proteoglycan matrix in the absence of FGF2. FGF2 treatment transformed some cells to fibroblast-like shapes and prominently suppressed expression of sulfated proteoglycan matrix. In the RCS cells treated with CNP or meclozine, the cellular shape remained round and the intensity of Alcian blue staining approximated that of FGF2-negative cells. Representative images of triplicated experiments are shown. Magnified images of the middle

panels are shown in the rightmost column. Bars in the left, middle, and right panels are 750, 150, and 30 μm, respectively. (D) Meclozine (20 μM) inhibited mRNA expression of matrix metalloproteinases in FGF2-treated RCS cells. Cells were treated with FGF2 and either CNP or meclozine for four hours and mRNAs were quantified by real-time RT-PCR. Expression levels of *Mmp10*, *Mmp13*, and *Adamts1* are presented as the mean and SD normalized to that of FGF2-negative cells ($n = 3$). FGF2-mediated increases of *Mmp10*, *Mmp13*, and *Adamts1* mRNA were antagonized by CNP and meclozine. Statistical significance is estimated by Student's t-test.
doi:10.1371/journal.pone.0081569.g001

RAF into RCS cells using lentivirus and quantified cell growth with the MTS assay. As predicted, meclozine ameliorated caMEK- and caRAF-mediated growth inhibition, whereas meclozine had no effect on caERK-mediated growth inhibition (Figure 5B). We observed the similar effects by counting cells (Figures S5). Both data point to a notion that meclozine is likely to inhibit MEK1/2-mediated ERK1/2 phosphorylation or activate phosphatase(s) for phosphorylated ERK1/2 (Figure 6).

Discussion

The drug repositioning strategy is an effort to identify new indications for the existing drugs. This strategy can potentially reduce the expenses and efforts associated with multi-stage testing of the hit compounds [20,23]. Among the 1,186 FDA-approved drugs that have favorable or validated pharmacokinetic and toxicological profiles, we identified meclozine as a novel inhibitor of the FGFR3 signaling, which can potentially be applied to clinical practice for short stature in FGFR3-related skeletal dysplasias. Meclozine is an over-the-counter H1 blocker, which has been safely used for motion sickness for more than 50 years. Because the optimal doses and adverse effects of meclozine have already been established, meclozine can be readily prescribed for FGFR3-related skeletal dysplasia after effectiveness in humans is confirmed.

Since there is no rational therapy for FGFR3-related disorders available to date, development of novel modalities to suppress the FGFR3 signaling has long been expected. Krejci et al. screened a library of 1,120 compounds and identified that NF449 inhibits FGFR3 signaling in RCS chondrocytes as well as in FGF2-treated embryonic bone organ culture. NF449 is structurally similar to suramin and possesses inhibitory activities of other tyrosine kinases in addition to FGFR3 [14]. Jonquoyet et al. identified that a

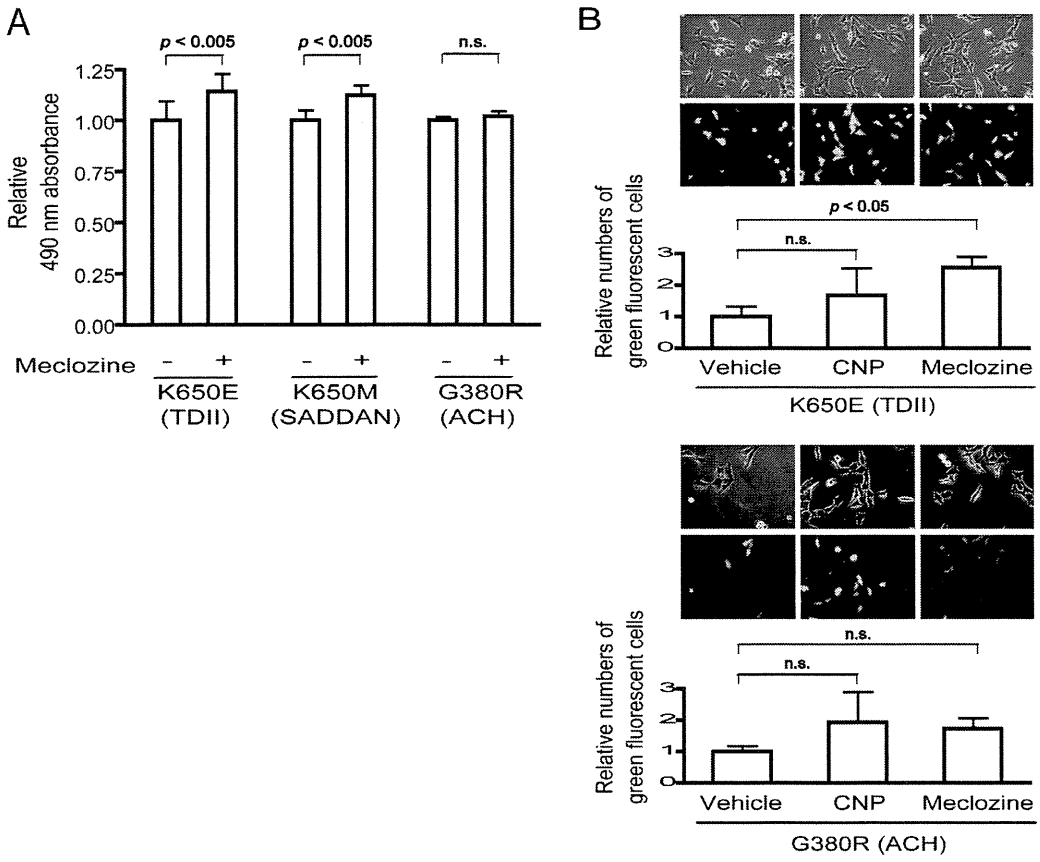

Figure 2. Meclozine mitigates abnormally suppressed proliferation of HCS-2/8 chondrocytes infected with lentivirus expressing mutant FGFR3. (A) HCS-2/8 cells expressing either FGFR3-K650E causing TDII, -K650M causing SADDAN, or G380R causing ACH were cultured with 20 μM meclozine for 48 hours and the proliferation was quantified by the MTS assay. Values are normalized to that without meclozine and the mean and SD are presented ($n = 12$). Meclozine ameliorated growth arrest driven by the mutations. (B) CNP (0.2 μM) and meclozine (20 μM) also alleviated K650E- and G380R-mediated growth inhibition visualized by Venus fluorescence expressed by the infected lentivirus. Fluorescence microscopy shows that the transfection efficiency is more than 90%. Both CNP and meclozine increased the Venus signal areas. Data are presented as the mean and SE that are normalized to that of vehicle ($n = 3$). Statistical significance is estimated by Student's t-test.
doi:10.1371/journal.pone.0081569.g002

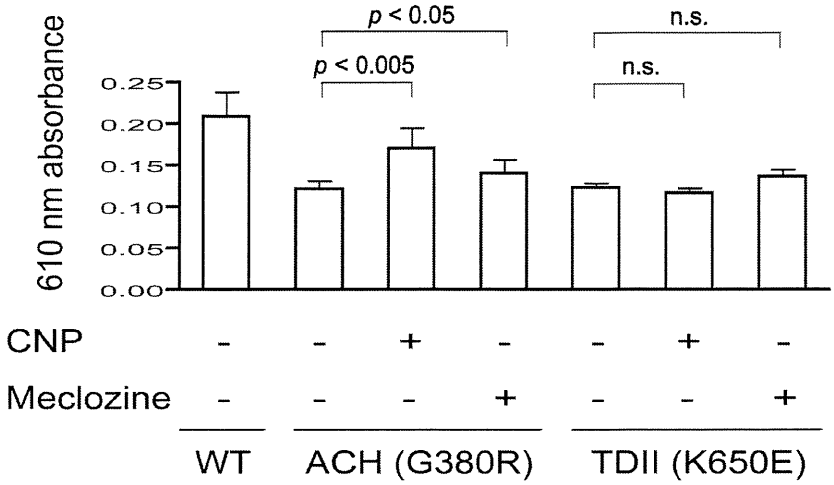

Figure 3. Meclozine facilitates chondrocyte differentiation of ATDC5 cells expressing mutant FGFR3 in micromass culture. ATDC5 cells were infected with lentivirus expressing FGFR3-WT (wild-type), FGFR3-G380R causing ACH, or FGFR3-K650E causing TDII. Similar expressions of the transgenes are shown by immunoblotting in Figure S3. ATDC5 cells in micromass culture were treated with CNP (0.2 μM) or meclozine (20 μM) for six days and were stained with Alcian blue. Experiments were repeated six times and representative images are shown. After staining, matrix proteoglycans in the cell lysate were quantified by measuring absorbance at 610 nm. The data are presented as the mean and SD ($n = 6$). CNP and meclozine increased the Alcian blue staining of ATDC5 cells expressing FGFR3-G380R and –K650E in micromass culture. Statistical significance is estimated by Student's t-test.
doi:10.1371/journal.pone.0081569.g003

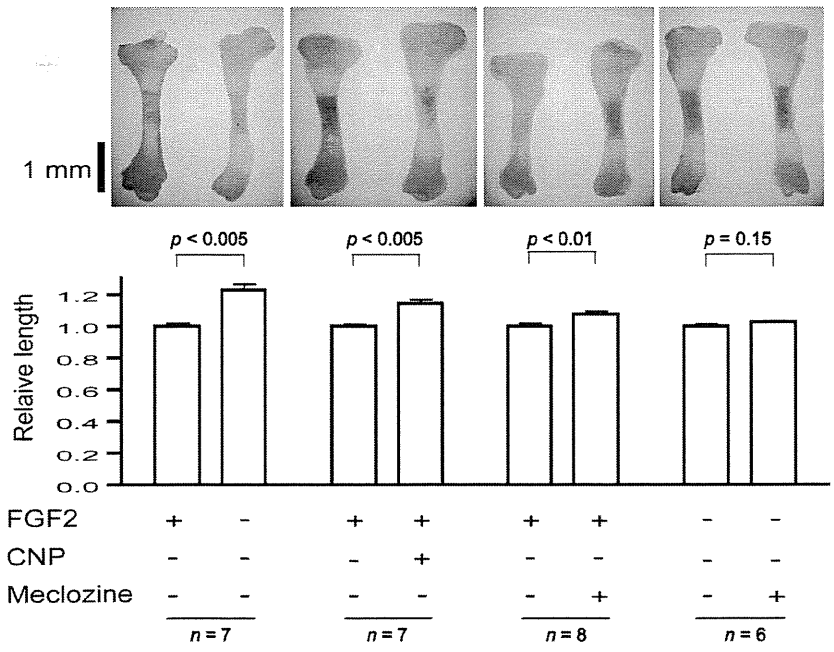

Figure 4. Meclozine increases the longitudinal length of embryonic tibiae with or without FGF2 treatment in bone explant culture. Unstained bilateral tibiae of the same individual were photographed side by side on day six of explant culture. Longitudinal bone lengths were normalized to that of untreated contralateral tibia, and the mean and SD are indicated. FGF2 causes inhibition of longitudinal bone growth. In the presence of FGF2, CNP (0.2 μM) and meclozine (20 μM) significantly increased the longitudinal length of embryonic tibiae. Even without FGF2, meclozine (20 μM) facilitated the growth of embryonic tibiae but without statistical significance (Student's t-test).
doi:10.1371/journal.pone.0081569.g004

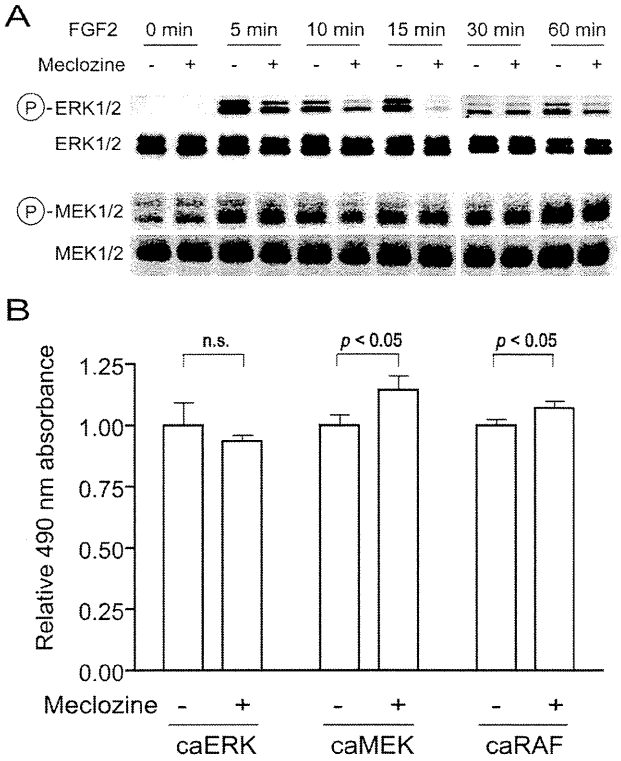

Figure 5. Meclozine attenuates FGFR3-mediated ERK phosphorylation in FGF2-treated RCS cells. (**A**) RCS cells were pretreated with 20 μM meclozine for 30 minutes before adding 5 ng/ml FGF2 and the levels of ERK and MEK phosphorylation were determined by Western blotting. As a loading control, the membranes were reprobed with antibodies against MEK and ERK. Meclozine suppressed FGF2-mediated ERK phosphorylation but not MEK phosphorylation after adding FGF2. (**B**) RCS cells were infected by lentivirus expressing constitutively active (ca) ERK, MEK, and RAF mutants. Cells were treated with 20 μM meclozine and their proliferation potencies were quantified using the MTS assay. The 490-nm absorbance was normalized to that without meclozine and the mean and SD are presented ($n = 3$). Meclozine rescued caMEK- and caRAF-mediated growth arrest, but had no effect on caERK-mediated growth arrest.
doi:10.1371/journal.pone.0081569.g005

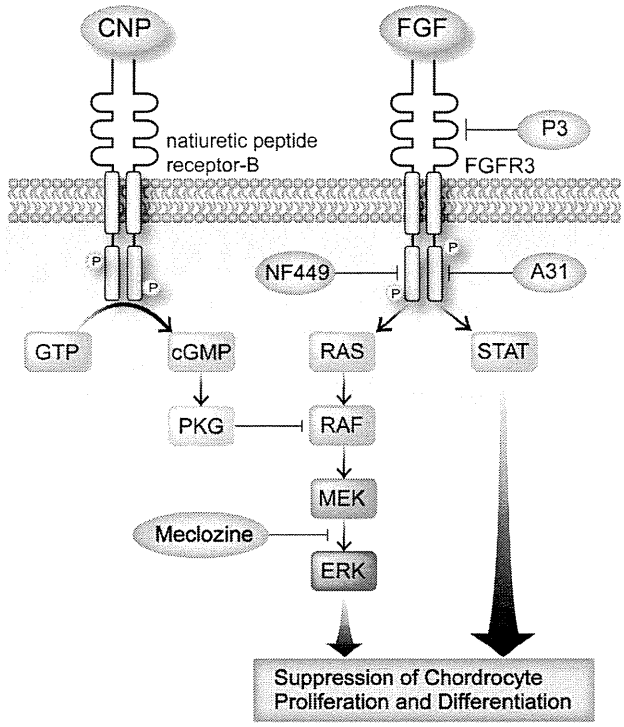

Figure 6. FGFR3 signal transduction in chondrocytes and mechanisms of FGFR3 inhibitors. Activations of MAPK (mitogen-activated protein kinase) and STAT (signal transducers and activators of transcription) negatively regulate chondrocyte proliferation and differentiation. MAPK signaling includes sequential stimulation of a signaling cascade involving RAS, RAF, MEK, and ERK. CNP binding to natriuretic peptide receptor-B induces the generation of the second messenger cGMP, which activates PKG and leads to attenuation of the MAPK pathway by inhibiting RAF activation. NF449 [14], A31 [16], and P3 [15] are recently identified FGFR3 inhibitors. NF449 and A31 have inhibitory effects on the kinase activity of FGFR3. P3 has an affinity for extracellular domain of FGFR3. Meclozine attenuates ERK phosphorylation.
doi:10.1371/journal.pone.0081569.g006

synthetic compound A31 is an inhibitor of the FGFR3 tyrosine kinase by *in silico* analysis. They demonstrated that A31 suppresses constitutive phosphorylation of FGFR3 and restores the size of embryonic femurs of *Fgfr3*$^{Y367C/+}$ mice in organ culture. In addition, A31 potentiates chondrocyte differentiation in the *Fgfr3*$^{Y367C/+}$ growth plate [16]. Jin et al. screened a library of random 12-peptide phages and found that P3 has a high and specific binding affinity for the extracellular domain of FGFR3. They showed that P3 promotes proliferation and chondrogenic differentiation of cultured ATDC5 cells, alleviates the bone growth retardation in bone rudiments from TD mice (*Fgfr3*$^{Neo\text{-}K644E/+}$ mice), and finally reversed the neonatal lethality of TD mice [15]. These novel FGFR3 tyrosine kinase inhibitors, however, may inhibit tyrosine kinases other than FGFR3 and may exert unexpected toxic effects in humans. Meclozine may also inhibit unpredicted tyrosine kinase pathways, but we can predict that there will be no overt adverse effect, because meclozine has been safely used for more than 50 years.

CNP is another therapeutic agent for FGFR3-related disorders. CNP-deficient mice were dwarfed with narrowing of the proliferative and hypertrophic zones of the growth plates [24]. Loss-of-function mutations in *NPR2* encoding a receptor for CNP are responsible for acromesomelic dysplasia Maroteaux-type (AMDM), a form of short-limbed human skeletal dysplasias [25]. Conversely, overexpression of CNP prevented the shortening of achondroplastic bones by inhibiting the MAPK signaling pathway [17]. Yasoda et al. demonstrated that continuous delivery of CNP through intravenous infusion successfully normalized the dwarfism of *Fgfr3*^{ach} mice [18]. As CNP has a very short half-life, Lorget et al. developed an extended plasma half-life CNP analog, BMN111, which is resistant to neutral-endopeptidase digestion [19]. They showed that subcutaneous administration of BMN111 exhibits a significant recovery of bone growth in *Fgfr3*$^{Y367C/+}$ mice. Meclozine showed a similar inhibitory activity on the FGFR3 signaling compared to CNP in *ex vivo* bone explant culture as well as *in vitro* chondrogenic cells. We expect that meclozine can be used as a substitute for or in addition to CNP and the CNP analog.

The MAPK pathway is one of the major signaling pathways of FGFR3 in proliferation and differentiation of chondrocytes. Sustained ERK activation in chondrocytes leads to decreased proliferation, increased matrix degradation, altered cell shape, and decreased differentiation [5,6]. CNP inhibits phosphorylation of RAF1 kinase through inhibition by PKGII [6,17]. We demonstrated that meclozine attenuates ERK phosphorylation in chondrocytes. Gohil et al. reported that meclozine has an anti-

oxidative phosphorylation (OXPHOS) activity in addition to anti-histamine and anti-muscarinic properties [26,27]. In their report, meclozine showed cytoprotective activities against ischemic injury in the brain and heart. Since other drugs with anti-histamine, anti-muscarinic, and anti-OXPHOS properties did not show inhibition of the FGFR3 signaling in our studies, pharmacological actions of meclozine on chondrogenesis are unlikely to be relevant to its anti-histamine, anti-muscarinic, or anti-OXPHOS properties. Although additional studies are required to prove that meclozine is indeed effective for patients with FGFR3-related skeletal dysplasias, we propose that meclozine is an attractive and potential therapeutic agent.

Materials and Methods

Screening of 1,186 FDA-approved compounds in rat chondrosarcoma (RCS) cells

RCS cells, which were kindly provided from Dr. Pavel Krejci (Medical Genetics Institute, Cedars-Sinai Medical Center, LA) [5], were cultured in Dulbecco's Modified Eagle's Medium (DMEM, Invitrogen) supplemented with 10% fetal bovine serum (FBS, Thermo Scientific) [14]. For the RCS growth arrest assays, $\sim 5 \times 10^3$ cells were seeded in a 96-well culture plate and incubated for 48 hours in the presence of 10 μM of 1,186 FDA-approved chemical compounds (Prestwick Chemical) and 5 ng/ml of FGF2 (R&D Systems). Cell proliferation was quantified by the MTS assay (Cell 96 AQueus One Solution Cell Proliferation Assay, Promega) according to the manufacturer's instructions. Cell numbers were counted using the TC 10 Automated Cell Counter (Bio-Rad). For counting cells, $\sim 1 \times 10^5$ cells were seeded in a 12-well culture plate and incubated for 48 hours in the presence of 10 or 20 μM of meclozine and 5 ng/ml of FGF2.

Alcian blue staining

For Alcian blue staining, $\sim 1 \times 10^5$ RCS cells in a 12-well plate were added with 5 ng/ml FGF2 and also with either 10 μM meclozine or 0.2 μM CNP (Calbiochem). After 72 hours, cells were fixed with methanol for 30 minutes at −20°C, and stained overnight with 0.5% Alcian Blue 8 GX (Sigma) in 1 N HCl. For quantitative analyses, Alcian blue-stained cells were lysed in 200 μl of 6 M guanidine HCl for 6 hours at room temperature [28]. The optical density of the extracted dye was measured at 610 nm using PowerScan 4 (DS Pharma Biomedical).

Total RNA extraction and real-time RT-PCR analysis

Total RNA was isolated from FGF2-treated RCS cells in the presence of 20 μM of meclozine or 0.2 μM of CNP using Trizol. The first strand cDNA was synthesized with ReverTra Ace (Toyobo). We quantified mRNA expression of matrix proteinases (*Mmp10*, *Mmp13*, and *Adamts1*) and extracellular matrix proteins (*Col2a1* and *Acan*) using LightCycler 480 Real-Time PCR (Roche) and SYBR Green (Takara). The mRNA levels were normalized for that of *Gapdh*.

Vectors and cell transfection

The pRK7-FGFR3-WT, -K650E, and -K650M vectors expressing wild-type and mutant FGFR3 [29] were kindly provided by Dr. Pavel Krejci (Medical Genetics Institute, Cedars-Sinai Medical Center, LA). The pRK7-FGFR3-G380R was constructed by the QuikChange site-directed mutagenesis kit (Stratagene). The wild-type and mutant *FGFR3* cDNAs were excised from pRK7-FGFR3 vectors by double digestion with *Hin*dIII and *Bam*HI. The lentivirus vector, CSII-CMV-MCS-IRES2-Venus, was kindly provided by Dr. Hiroyuki Miyoshi (Riken BioResource Center, Tsukuba, Japan.), and was digested with *Nhe*I and *Bam*HI. The *Hin*dIII site of the insert and the *Nhe*I site of the vector were blunted using Quick Blunting Kit (New England Biolabs) before ligation. HEK293 cells were plated in a 150-mm dish on the day before transfection. We introduced the pLP1, pLP2, pLP/VSVG plasmids (ViraPower Packaging Mix, Invitrogen), and the CSII-CMV-MCS-IRES2-Venus vector into HEK293 cells with Lipofectamine 2000 (Invitrogen) according to the manufacturer's protocols. At 48 hours after transfection, we filtered the media containing the virus particles using the Millex-HV 0.45 μm PVDF filters (Millex) and purified lentivirus using two steps of ultracentrifugation (Beckman Coulter). The lentivirus was added to the medium of HCS-2/8 or ATDC5 cells. After 48 hours, we confirmed that more than 90% of cells were positive for Venus signals.

Clones that express constitutively active mutants in the MAPK/ERK pathway, pcDNA4Myc-ERK2(PD), pcDNA3HA-MEK1(DD), and pcDNA3Flag-C-rafΔN [30], were kindly provided by Dr. Mutsuhiro Takekawa (Medical Science Institute, Tokyo University, Japan). The inserts were digested with *Bam*HI and *Xho*I, and were cloned into the CSII-CMV-MCS-IRES2-Venus at the *Bam*HI sites after blunting all digested ends. Lentivirus particles were generated as described above and were used to infect RCS cells.

Growth assay of human chondrosarcoma (HCS-2/8) cells

HCS-2/8 chondrocytic cells were kindly provided by Dr. Masaharu Takigawa [31]. The ethical review committee of Nagoya University Graduate School of Medicine approved the use of HCS-2/8 cells in condition that we do not analyze the whole genome of HCS-2/8 cells. HCS-2/8 cells were seeded in a 96-well tissue culture plate. HCS-2/8 cells were then infected with lentivirus expressing either FGFR3-WT, -K650E, -K650M, or G380R. After 48 hours, the numbers of cells were estimated by the MTS assay. In addition, $\sim 1 \times 10^5$ HCS-2/8 cells in a 12-well tissue plate were introduced with lentivirus expressing FGFR3-G380R, or -K650E. After 72 hours, the Venus-positive cell areas were quantified by the ArrayScan VTI HCS Reader (Thermo Scientific).

Micromass culture of ATDC5 cells

Mouse embryonic carcinoma-derived ATDC5 cells [32] were infected with lentivirus expressing either FGFR3-WT, -G380R, or -K650E. The infected ATDC5 cells were subjected to micromass cultures as described previously [33]. Briefly, ATDC5 cells were suspended in DMEM/F-12 (1:1) medium (Sigma) containing 5% FBS at a density of 1×10^7 cells/ml and plated in 10-μl droplets to simulate the high-density chondrogenic condensations. After 1-hour incubation, the same medium supplemented with 1% insulin-transferrin-sodium selenite (ITS, Sigma) was added to the cells. Medium was changed every other day until harvesting cells on day 6.

Bone explant culture

The animal study was approved by the Animal Care and Use Committee of the Nagoya University Graduate School of Medicine. For bone explant culture, tibiae were dissected under the microscope from wild-type ICR mouse embryos on E16.5 (Japan SLC), placed in a 48-well plate, and cultured in BGJb medium (Invitrogen) supplemented with 0.2% bovine serum albumin and 150 μg/ml ascorbic acid. The medium was changed everyday. Embryonic tibiae were further treated with 100 ng/ml FGF2 in the presence or absence of 20 μM meclozine or 0.2 μM CNP for 6 days, then photographed and fixed in 10% formaldehyde in phosphate-buffered saline, demineralized with 0.5 M EDTA, and embedded in paraffin. Sections were stained with hematoxylin-eosin and Alcian blue. Images were taken with

the SZ61 microscope (Olympus) equipped with the XZ-1 digital camera (Olympus). The longitudinal length of bone, which was defined as the length between proximal and distal articular cartilage, was measured using ImageJ (NIH).

Western blotting and signaling studies

RCS cells were treated with or without 20 μM meclozine for 30 min before adding 5 ng/ml FGF2. After 0 to 60 min, cells were lysed in the ice-cold RIPA Lysis Buffer (Santa Cruz) supplemented with proteinase inhibitors. Whole cell lysates were separated on SDS-PAGE and transferred to a nitrocellulose membrane. The phosphorylation levels of molecules in the MAPK pathway were determined by Western blotting using the following antibodies: ERK1/2 (L34F12), phospho-ERK1/2(Thr^{202}/Tyr^{204}) (D13.14.4E), MEK1/2 (L38C12), and phospho-MEK1/2(Ser$^{217/221}$) (41G9) purchased from Cell Signaling.

The expressions of the introduced wild-type and mutant FGFR3 constructs in HCS-2/8 and ATDC5 cells were determined by Western blotting using antibodies for FGFR3 (sc123, Santa Cruz) and GFP (11814460001, Roche).

Supporting Information

Figure S1 Expression levels of *Col2a1 and Acan* mRNAs were unchanged in FGF2-treated RCS cells. Cells were treated with FGF2 for 72 hours and mRNAs were quantified by real-time RT-PCR. Expression levels of *Col2a1* and *Acan* mRNAs are presented as the mean and SD normalized to that of FGF2-negative cells ($n = 3$). FGF2 minimally suppressed the *Acan* expression but without statistical significance (Student's t-test).
(TIF)

Figure S2 K650E-expressing HCS-2/8 cells showed suppressed cellular proliferation. (**A**) Proliferation of HCS-2/8 cells infected with lentivirus expressing either FGFR3-WT (wild-type) or FGFR3-K650E (TDII) was quantified using the MTS assay at 48 hours after seeding. The growth of HCS-2/8 cells expressing FGFR3-K650E was significantly less than that of FGFR3-WT ($p<0.001$). The mean and SD are plotted. (**B**) Immunoblotting of FGFR3 and Venus to showing efficient expressions of FGFR3-WT and FGFR3-K650E in HCS-2/8 cells. FGFR3 is transcribed by CMV and Venus is downstream of IRES2 on the same transcript. As a control, the membrane was reprobed with Venus by anti-GFP antibody.
(TIF)

Figure S3 Immunoblotting of FGFR3 showing efficient expressions of FGFR3-WT, -G380R, and -K650E in ATDC5 cells. ATDC5 cells were infected with lentivirus expressing FGFR3-WT (wild-type), -G380R (ACH), and -K650E (TDII). FGFR3 is transcribed by CMV and Venus is downstream of IRES2 on the same transcript. As a control, the membrane was reprobed with Venus by anti-GFP antibody.
(TIF)

Figure S4 Meclozine increases the thickness of embryonic tibial growth plate in FGF2-treated bone explant culture. Tibia sections were stained with hematoxylin-eosin and Alcian blue on day six of explant culture. Arrows indicate hypertrophic chondrocyte layers. FGF2 treatment reduced the thickness of the layer, while treatments with CNP and meclozine mitigated the effect of FGF2.
(TIF)

Figure S5 Meclozine attenuates FGFR3-mediated ERK phosphorylation in FGF2-treated RCS cells. RCS cells were infected by lentivirus expressing constitutively active (ca) ERK, MEK, and RAF mutants. Cells were treated with 20 μM meclozine and the cell numbers were counted. The cell numbers were normalized to that without meclozine and the mean and SD are presented ($n = 6$). Meclozine rescued caMEK-mediated, but not caERK-mediated, growth arrest, although no statistical significance was observed.
(TIF)

Acknowledgments

We would like to thank Dr. Pavel Krejci at Cedars-Sinai Medical Center for providing pRK7-FGFR3-WT, -K650E, and -K650M vectors, as well as RCS cells; Dr. Masaharu Takigawa at Okayama University for providing HCS-2/8 cells; Dr. Mutsuhiro Takekawa at Tokyo University for providing pcDNA4Myc-ERK2(PD), pcDNA3HA-MEK1(DD), and pcDNA3Flag-C-rafΔN; and Drs. Hiroyuki Miyoshi and Atsuhi Miyawaki at Riken BioResource Center for providing CSII-CMV-MCS-IRES2-Venus lentivirus vector. We also thank Keiko Itano for technical assistance.

Author Contributions

Conceived and designed the experiments: H. Kitoh NI KO. Performed the experiments: MM KM H. Kaneko. Analyzed the data: MM BO MI AM. Wrote the paper: MM H. Kitoh KO.

References

1. Waller DK, Correa A, Vo TM, Wang Y, Hobbs C, et al. (2008) The population-based prevalence of achondroplasia and thanatophoric dysplasia in selected regions of the US. Am J Med Genet A 146A: 2385–2389.
2. Horton WA, Hall JG, Hecht JT (2007) Achondroplasia. Lancet 370: 162–172.
3. Rousseau F, Bonaventure J, Legeai-Mallet L, Pelet A, Rozet JM, et al. (1994) Mutations in the gene encoding fibroblast growth factor receptor-3 in achondroplasia. Nature 371: 252–254.
4. Shiang R, Thompson LM, Zhu YZ, Church DM, Fielder TJ, et al. (1994) Mutations in the transmembrane domain of FGFR3 cause the most common genetic form of dwarfism, achondroplasia. Cell 78: 335–342.
5. Krejci P, Bryja V, Pachernik J, Hampl A, Pogue R, et al. (2004) FGF2 inhibits proliferation and alters the cartilage-like phenotype of RCS cells. Exp Cell Res 297: 152–164.
6. Krejci P, Masri B, Fontaine V, Mekikian PB, Weis M, et al. (2005) Interaction of fibroblast growth factor and C-natriuretic peptide signaling in regulation of chondrocyte proliferation and extracellular matrix homeostasis. J Cell Sci 118: 5089–5100.
7. Murakami S, Balmes G, McKinney S, Zhang Z, Givol D, et al. (2004) Constitutive activation of MEK1 in chondrocytes causes Stat1-independent achondroplasia-like dwarfism and rescues the Fgfr3-deficient mouse phenotype. Genes Dev 18: 290–305.
8. Prinos P, Costa T, Sommer A, Kilpatrick MW, Tsipouras P (1995) A common FGFR3 gene mutation in hypochondroplasia. Hum Mol Genet 4: 2097–2101.
9. Tavormina PL, Bellus GA, Webster MK, Bamshad MJ, Fraley AE, et al. (1999) A novel skeletal dysplasia with developmental delay and acanthosis nigricans is caused by a Lys650Met mutation in the fibroblast growth factor receptor 3 gene. Am J Hum Genet 64: 722–731.
10. Tavormina PL, Shiang R, Thompson LM, Zhu YZ, Wilkin DJ, et al. (1995) Thanatophoric dysplasia (types I and II) caused by distinct mutations in fibroblast growth factor receptor 3. Nat Genet 9: 321–328.
11. Toydemir RM, Brassington AE, Bayrak-Toydemir P, Krakowiak PA, Jorde LB, et al. (2006) A novel mutation in FGFR3 causes camptodactyly, tall stature, and hearing loss (CATSHL) syndrome. Am J Hum Genet 79: 935–941.
12. Beever JE, Smit MA, Meyers SN, Hadfield TS, Bottema C, et al. (2006) A single-base change in the tyrosine kinase II domain of ovine FGFR3 causes hereditary chondrodysplasia in sheep. Anim Genet 37: 66–71.
13. Horton WA, Hecht JT, Hood OJ, Marshall RN, Moore WV, et al. (1992) Growth hormone therapy in achondroplasia. Am J Med Genet 42: 667–670.
14. Krejci P, Murakami S, Prochazkova J, Trantirek L, Chlebova K, et al. (2010) NF449 is a novel inhibitor of fibroblast growth factor receptor 3 (FGFR3) signaling active in chondrocytes and multiple myeloma cells. J Biol Chem 285: 20644–20653.

15. Jin M, Yu Y, Qi H, Xie Y, Su N, et al. (2012) A novel FGFR3-binding peptide inhibits FGFR3 signaling and reverses the lethal phenotype of mice mimicking human thanatophoric dysplasia. Hum Mol Genet 21: 5443–5455.
16. Jonquoy A, Mugniery E, Benoist-Lasselin C, Kaci N, Le Corre L, et al. (2012) A novel tyrosine kinase inhibitor restores chondrocyte differentiation and promotes bone growth in a gain-of-function Fgfr3 mouse model. Hum Mol Genet 21: 841–851.
17. Yasoda A, Komatsu Y, Chusho H, Miyazawa T, Ozasa A, et al. (2004) Overexpression of CNP in chondrocytes rescues achondroplasia through a MAPK-dependent pathway. Nat Med 10: 80–86.
18. Yasoda A, Kitamura H, Fujii T, Kondo E, Murao N, et al. (2009) Systemic administration of C-type natriuretic peptide as a novel therapeutic strategy for skeletal dysplasias. Endocrinology 150: 3138–3144.
19. Lorget F, Kaci N, Peng J, Benoist-Lasselin C, Mugniery E, et al. (2012) Evaluation of the therapeutic potential of a CNP analog in a Fgfr3 mouse model recapitulating achondroplasia. Am J Hum Genet 91: 1108–1114.
20. Abbott A (2002) Neurologists strike gold in drug screen effort. Nature 417: 109.
21. Bian Y, Masuda A, Matsuura T, Ito M, Okushin K, et al. (2009) Tannic acid facilitates expression of the polypyrimidine tract binding protein and alleviates deleterious inclusion of CHRNA1 exon P3A due to an hnRNP H-disrupting mutation in congenital myasthenic syndrome. Hum Mol Genet 18: 1229–1237.
22. Dailey L, Laplantine E, Priore R, Basilico C (2003) A network of transcriptional and signaling events is activated by FGF to induce chondrocyte growth arrest and differentiation. J Cell Biol 161: 1053–1066.
23. Heemskerk J, Tobin AJ, Bain LJ (2002) Teaching old drugs new tricks. Meeting of the Neurodegeneration Drug Screening Consortium, 7-8 April 2002, Washington, DC, USA. Trends Neurosci 25: 494–496.
24. Chusho H, Tamura N, Ogawa Y, Yasoda A, Suda M, et al. (2001) Dwarfism and early death in mice lacking C-type natriuretic peptide. Proc Natl Acad Sci U S A 98: 4016–4021.
25. Bartels CF, Bukulmez H, Padayatti P, Rhee DK, van Ravenswaaij-Arts C, et al. (2004) Mutations in the transmembrane natriuretic peptide receptor NPR-B impair skeletal growth and cause acromesomelic dysplasia, type Maroteaux. Am J Hum Genet 75: 27–34.
26. Gohil VM, Sheth SA, Nilsson R, Wojtovich AP, Lee JH, et al. (2010) Nutrient-sensitized screening for drugs that shift energy metabolism from mitochondrial respiration to glycolysis. Nat Biotechnol 28: 249–255.
27. Gohil VM, Offner N, Walker JA, Sheth SA, Fossale E, et al. (2011) Meclizine is neuroprotective in models of Huntington's disease. Hum Mol Genet 20: 294–300.
28. De Bari C, Dell'Accio F, Luyten FP (2001) Human periosteum-derived cells maintain phenotypic stability and chondrogenic potential throughout expansion regardless of donor age. Arthritis Rheum 44: 85–95.
29. Krejci P, Masri B, Salazar L, Farrington-Rock C, Prats H, et al. (2007) Bisindolylmaleimide I suppresses fibroblast growth factor-mediated activation of Erk MAP kinase in chondrocytes by preventing Shp2 association with the Frs2 and Gab1 adaptor proteins. J Biol Chem 282: 2929–2936.
30. Emrick MA, Hoofnagle AN, Miller AS, Ten Eyck LF, Ahn NG (2001) Constitutive activation of extracellular signal-regulated kinase 2 by synergistic point mutations. J Biol Chem 276: 46469–46479.
31. Takigawa M, Tajima K, Pan HO, Enomoto M, Kinoshita A, et al. (1989) Establishment of a clonal human chondrosarcoma cell line with cartilage phenotypes. Cancer Res 49: 3996–4002.
32. Atsumi T, Miwa Y, Kimata K, Ikawa Y (1990) A chondrogenic cell line derived from a differentiating culture of AT805 teratocarcinoma cells. Cell Differ Dev 30: 109–116.
33. Hoogendam J, Parlevliet E, Miclea R, Lowik CW, Wit JM, et al. (2006) Novel early target genes of parathyroid hormone-related peptide in chondrocytes. Endocrinology 147: 3141–3152.

Human Molecular Genetics, 2014, Vol. 23, No. 7 **1856–1868**
doi:10.1093/hmg/ddt578
Advance Access published on November 13, 2013

LRP4 third β-propeller domain mutations cause novel congenital myasthenia by compromising agrin-mediated MuSK signaling in a position-specific manner

Bisei Ohkawara[1], Macarena Cabrera-Serrano[3], Tomohiko Nakata[1], Margherita Milone[3], Nobuyuki Asai[1], Kenyu Ito[1], Mikako Ito[1], Akio Masuda[1], Yasutomo Ito[2], Andrew G. Engel[3,*] and Kinji Ohno[1,*]

[1]Division of Neurogenetics, Center for Neurological Diseases and Cancer and [2]Division for Medical Research Engineering, Nagoya University Graduate School of Medicine, Nagoya, Japan [3]Department of Neurology, Mayo Clinic, Rochester, MN, USA

Received June 10, 2013; Revised October 15, 2013; Accepted November 11, 2013

Congenital myasthenic syndromes (CMS) are heterogeneous disorders in which the safety margin of neuromuscular transmission is compromised by one or more specific mechanisms. Using Sanger and exome sequencing in a CMS patient, we identified two heteroallelic mutations, p.Glu1233Lys and p.Arg1277His, in *LRP4* coding for the postsynaptic low-density lipoprotein receptor-related protein 4. LRP4, expressed on the surface of the postsynaptic membrane of the neuromuscular junction, is a receptor for neurally secreted agrin, and LRP4 bound by agrin activates MuSK. Activated MuSK in concert with Dok-7 stimulates rapsyn to concentrate and anchor AChR on the postsynaptic membrane and interacts with other proteins implicated in the assembly and maintenance of the neuromuscular junction. LRP4 also functions as an inhibitor of Wnt/beta-catenin signaling. The identified mutations in *LRP4* are located at the edge of its 3rd beta-propeller domain and decrease binding affinity of LRP4 for both MuSK and agrin. Mutations in the LRP4 3rd beta-propeller domain were previously reported to impair Wnt signaling and cause bone diseases including Cenani–Lenz syndactyly syndrome and sclerosteosis-2. By analyzing naturally occurring and artificially introduced mutations in the LRP4 3rd beta-propeller domain, we show that the edge of the domain regulates the MuSK signaling whereas its central cavity governs Wnt signaling. We conclude that *LRP4* is a new CMS disease gene and that the 3rd beta propeller domain of LRP4 mediates the two signaling pathways in a position-specific manner.

INTRODUCTION

Congenital myasthenic syndromes (CMS) are diverse disorders in which the safety margin of neuromuscular transmission is compromised by deficiency or abnormal function of an endplate (EP)-associated protein. To date, mutations in no fewer than 17 genes coding for proteins expressed at EP are known to cause CMS (1): *ALG2* (MIM 607905), *ALG14* (MIM 612866), *CHRNA1* (MIM 100690), *CHRNB1* (MIM 100710), *CHRND* (MIM 100720), *CHRNE* (MIM 100725), *AGRN* (MIM 103320), *CHAT* (MIM 118491), *DPAGT1* (MIM 191350), *GFPT1* (MIM 138292), *LAMB2* (MIM 150325), *PLEC* (MIM 601282), *MUSK* (MIM 601296), *RAPSN* (MIM 601592), *COLQ* (MIM 603033), *SCN4A* (MIM 603967) and *DOK7* (MIM 610285). We here describe our findings in a novel CMS caused by mutations in the low-density lipoprotein receptor-related protein 4 encoded by *LRP4*.

EP development is triggered by the binding of agrin released from the nerve terminal to LRP4, a transmembrane protein of the

*To whom correspondence should be addressed at: Division of Neurogenetics, Center for Neurological Diseases and Cancer, Nagoya University Graduate School of Medicine, 65 Tsurumai, Showa-ku, Nagoya, Aichi 466-8550, Japan. Tel: +81 52 744 2446; Fax: +81 52 744 2449; Email: ohnok@med.nagoya-u.ac.jp (K.O.); Neuromuscular Research Laboratory, Department of Neurology, Mayo Clinic, 200 First Street SW, Rochester, MN 55905, USA. Tel: +1 507 284 5102; Fax: +1 507 2845831; Email: age@mayo.edu (A.G.E.)

postsynaptic membrane (2,3). LRP4 bound to agrin forms a ternary complex with the postsynaptic transmembrane muscle-specific receptor tyrosine kinase (MuSK). In this complex, the 3rd β-propeller domain of LRP4 is important for association with MuSK (4), although the interacting conformations remain unresolved. Binding of LRP4 to MuSK triggers phosphorylation and activation of the MuSK intracellular kinase domain. Activated MuSK in concert with Dok-7 stimulates rapsyn to concentrate and anchor AChR in the postsynaptic membrane and to interact with other proteins implicated in the assembly and maintenance of the NMJ (5). LRP4 was recently reported to provide a retrograde signal for presynaptic differentiation at neuromuscular junction (6,7). In addition, autoantibodies directed against LRP4 were recently recognized to cause a form of autoimmune myasthenia gravis (8–10).

In addition to its specific role at the NMJ, LRP4 is also a well-characterized inhibitor of the Wnt-signaling pathway. LRP4 signaling is involved in skeleton formation and kidney development. Mutations in *LRP4* have been reported in Cenani–Lenz syndactyly syndrome (CLSS) (11), sclerosteosis-2 (12), and low bone mineral density in human (13) and mice (14). Similarly, *Lrp4* mutations cause mule foot disease in cow (15) and kidney and limb defects in mouse (16). In addition, a missense SNP rs2306029 in *LRP4* is associated with 4.17-fold increase in the risk of developing Richter syndrome (17). To date, no report has implicated *LRP4* as a CMS disease gene.

Using Sanger and exome-capture resequencing, we identified two heteroallelic missense variants in *LRP4*, p.Glu1233Lys (c.3697G > A) and p.Arg1277His (c.3830G > A). Both variants are located at the edge of the 3rd β-propeller domain of LRP4. We show that each variant impairs binding ability of LRP4 for both agrin and MuSK as well as subsequent agrin-mediated phosphorylation and activation of MuSK, but neither mutation affects the Wnt-signaling pathway. Finally, by analysis of mutations in other diseases and by examining effects of artificially engineered mutations into the 3rd LRP4 β-propeller domain, we show the edge of this domain mediates the MuSK signaling, whereas its central cavity mediates the Wnt signaling.

RESULTS

Clinical data

The patient was born after 42 weeks of gestation with fetal distress and with Apgar scores of 3 and 6 at 1 and 5 min, respectively. Immediately after birth, she had a respiratory arrest and required hospitalization for feeding and respiratory support until the age of 6 months. She started to walk at 18 months but could only walk short distances. During childhood, she fatigued abnormally, could not climb step and was partially wheelchair dependent. Examination at the Mayo Clinic at ages 9 and 14 years revealed mild eyelid ptosis, slight limitation of lateral eye movements, moderately severe proximal greater than distal muscle weakness and hypoactive tendon reflexes. Repetitive nerve stimulation of the spinal accessory nerve showed a 13–16% decrement of the fourth compared with the first compound muscle action potential evoked from the trapezius, biceps and rectus femoris muscles with no significant decrement in the anterior tibial muscle. The decremental responses were transiently improved by edrophonium chloride, a fast acting cholinergic agonist. However, therapy for a few days with pyridostigmine at age 12 markedly worsened the patient's weakness. There was no history of similarly affected family members.

Endplate studies

An intercostal muscle specimen was obtained from the patient at age 17 years. Routine histologic examination revealed type 1 fiber preponderance. Synaptic contacts, examined in face-on views of glutaraldehyde-fixed AChE-reacted teased muscle fibers revealed multiple irregularly arrayed synaptic contacts that varied in shape and size (Fig. 1). None of the EPs had a normal pretzel shape. Electron microscopy examination of 54 EP regions of 29 EPs showed that the structural integrity of the nerve terminals and postsynaptic regions was preserved but quantitative analysis revealed that the size of the nerve terminals was reduced to 60%, and that of the postsynaptic region to 48%, of the corresponding control value (Table 1).

Immunofluorescence microscopy examination of frozen sections revealed normal expression of AChR and AChE at patient EPs. Ultrastructural localization of AChR at the EPs with peroxidase-labeled α-bungarotoxin (bgt) demonstrated normal distribution and density of AChR on the junctional folds. However, the total number of AChRs per EP fell slightly below the range of control values (Table 1).

The MEPP amplitude and the number of quanta released by nerve impulse fell in the normal range, and patch-clamp recordings from10 EPs revealed normal kinetics of the AChR channel (data not shown).

Sanger and exome-capture resequencing analysis

We analyzed the patient DNA using the exome-capture resequencing analysis. The number of SOLiD tags was 90.7×10^6

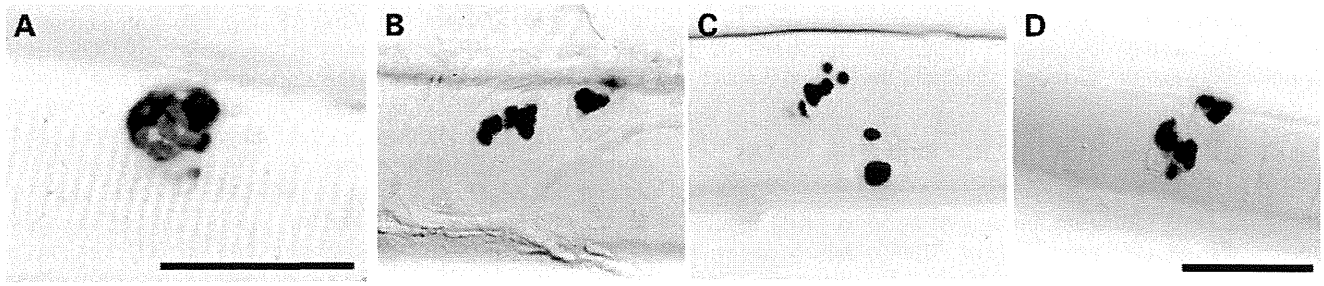

Figure 1. Synaptic contacts in intercostal muscle visualized by the cholinesterase reaction. (**A**) Normal EP. (**B–D**) Patient EPs. Note irregularly arrayed pleomorphic synaptic contacts at patient EPs. Bar in (A) indicates 50 μm. Bar in (D) indicates 50 μm for panels (B–D).

Table 1. Quantitative analysis of EP ultrastructure and [^{125}I]α-bungarotoxin-binding sites per EP

	Patient	Controls	*P*-value
Nerve terminal area (μm^2)	2.45 ± 0.30 (54)	3.88 ± 0.39 (63)	<0.005
Postsynaptic area (μm^2)	5.51 ± 0.45 (54)	10.6 ± 0.79 (59)	<0.001
[^{125}I]α-bgt-binding sites/EP	8.7×10^6	$12.82 \pm 0.79 \times 10^6$ (13) Range: 9.3–18.7	

Values represent mean ± SE. More than one region can occur at an EP. Values in parenthesis represent number of EP regions except for [^{125}I]α-bgt-binding sites where they indicate number of subjects. *P*-values are based on *t*-test.

spanning 4.53 Gb, and 72.8×10^6 tags (80.2%) spanning 3.47 Gb (76.6%) were mapped to the human genome hg19/GRCh37. As the SureSelect probes span 38 Mb, the mean coverage became 91.4. Among the 38-Mb SureSelect probe regions, 3.9% of nucleotides were not covered by any tags. Search for SNVs and indels using Avadis NGS with default parameters detected 46 555 SNVs/indels. We eliminated SNVs/indels registered in dbSNP137 and those with unreliable calls (Avadis decibel score ≤200), and obtained 4074 SNVs/indels. Restriction of our analysis to non-synonymous, frameshifting and splicing SNVs/indels in 33 candidate genes that are essential for the neuromuscular signal transmission yielded three SNVs. Among the three SNVs, a heterozygous c.1148C > G SNV predicting p.Ser376Arg in *SNTB2* encoding syntrophin β_2 was observed in a patient with periodic paralysis among our cohort of 31 patients other than CMS. In addition, 13 other missense SNPs and two frameshifting SNPs are registered in 539 codons encoded by *SNTB2* in dbSNP137. Thus, p.Ser376Arg in *SNTB2* was unlikely to be pathogenic. The two other SNVs were heterozygous c.3697G > A (chr11: 46 897 357) and c.3830G > A (chr11: 46 897 102) in *LRP4*, which predicted p.Glu1233Lys (EK mutation) and p.Arg1277His (RH mutation), respectively. Sanger sequencing of the patient's genomic DNA and mRNA confirmed both mutations and sequencing of cloned mRNA indicated that the mutations were heteroallelic. The father was heterozygous for p.Glu1233Lys. A half brother carried no mutation. No DNA was available from the mother. According to the PolyPhen-2 (18), SIFT (19) and Mutation Taster (20) algorithms, the predicted consequences of the EK mutation were 'benign', 'tolerated' and 'disease causing with $P > 0.99999$', respectively. Those of the RH mutation were 'probably damaging', 'affect protein function' and 'disease causing with $P > 0.99999$', respectively. LRP4 is a transmembrane protein with large extracellular domains (Fig. 2A). These mutations were in the 3rd low-density lipoprotein receptor (LDLR) type B repeat, known as β-propeller-like structure. The EK and RH mutations are downstream of the 4th and 5th YWTD motifs, respectively (Fig. 2B). The YWTD motifs are predicted to form the second β sheet below the surface β sheet of each blade of the 3rd β-propeller domain, and the mutations are at the linker between the surface β sheet and the second β sheet.

The EK and RH mutations in *LRP4* impair the MuSK signaling pathway

During the NMJ formation, binding of agrin to LRP4 induces phosphorylation and activation of MuSK, which activates ATF2 downstream of JNK and induces clustering of AChR. To study effects of the mutations in this signaling pathway, we used a JNK-responsive ATF2-luciferase (ATF2-luc) reporter (21), which specifically monitors MuSK-dependent stimulation in transfected HEK293 cells. Overexpression of LRP4 and MuSK activated the ATF2-luc reporter in the absence of agrin, as previously reported (22). The EK mutant minimally and the RH mutant moderately impaired LRP4-induced activation of ATF2-luc (Fig. 3A). Addition of agrin to the medium markedly enhanced the ATF2-luc activity for the wild-type LRP4, whereas both mutants completely abolished responsiveness to agrin (Fig. 3A).

We also examined effects of the mutations on MuSK phosphorylation that occurs immediately after formation of the agrin/LRP4/MuSK complex. Consistent with its effects on the signaling activity, agrin enhanced MuSK phosphorylation in the presence of wild-type LRP4 but not in the presence of mutant LRP4 in HEK293 cells (Fig. 3B) and in Lrp4-downregulated C2C12 myoblasts (Fig. 4B). Similarly, wild-type LRP4, but not EK and RH mutants, rescued AChR clustering in Lrp4-downregulated C2C12 myotubes (Fig. 4C). These results support the notion that the EK and RH mutations compromise agrin-mediated activation of MuSK and AChR clustering.

LRP4 has also been known as an extracellular antagonist for Wnt signaling. Wnt signaling is involved in tissue development including limb, bone and kidney. Indeed, previously reported mutations of *LRP4* in human, mouse and cow exhibit structural abnormalities in limb, bone and/or kidney. We thus examined the effects of our LRP4 mutations on Wnt-signaling pathway using the TOPFLASH reporter. Wild-type LRP4 suppressed the Wnt3a-mediated TOPFLASH activity, and the EK and RH mutations retained similar suppressive effects (Fig. 3C). Lack of limb, bone and kidney symptoms in our patient can be attributed to EK and RH only affecting agrin-induced activation of MuSK but having no effect on Wnt signaling.

LRP4 directly binds to agrin and MuSK through its extracellular domain. To test the effects of the LRP4 mutations on binding to MuSK and agrin, we performed cell surface-binding assays. We first confirmed that the EK and RH mutants had no effect on LRP4 expressions in cell body and cell membrane in COS7 cells (Supplementary Material, Fig. S1). MuSKect-mycAP (Fig. 5A) and agrin-mycAP (Fig. 5B) bound efficiently to wild-type LRP4 expressed on the surface of COS7 cells. The RH and EK mutants compromised binding of both MuSKect-mycAP and agrin-mycAP (Fig. 5A and B). We also analyzed direct binding of LRP4ecd-Flag to purified MuSKect-mycAP (Fig. 5C) and agrin-mycAP (Fig. 5D) by *in vitro* plate-binding assays (Fig. 5E and F). We found that the mutations decreased binding affinities of LRP4 for agrin-mycAP (Fig. 5E) and MuSKect-mycAP (Fig. 5F). The RH mutant compromised binding of agrin and MuSK more than the EK mutant in the cell surface-binding assay but not in the *in vitro* plate-binding assay, which may be accounted for by some other molecules

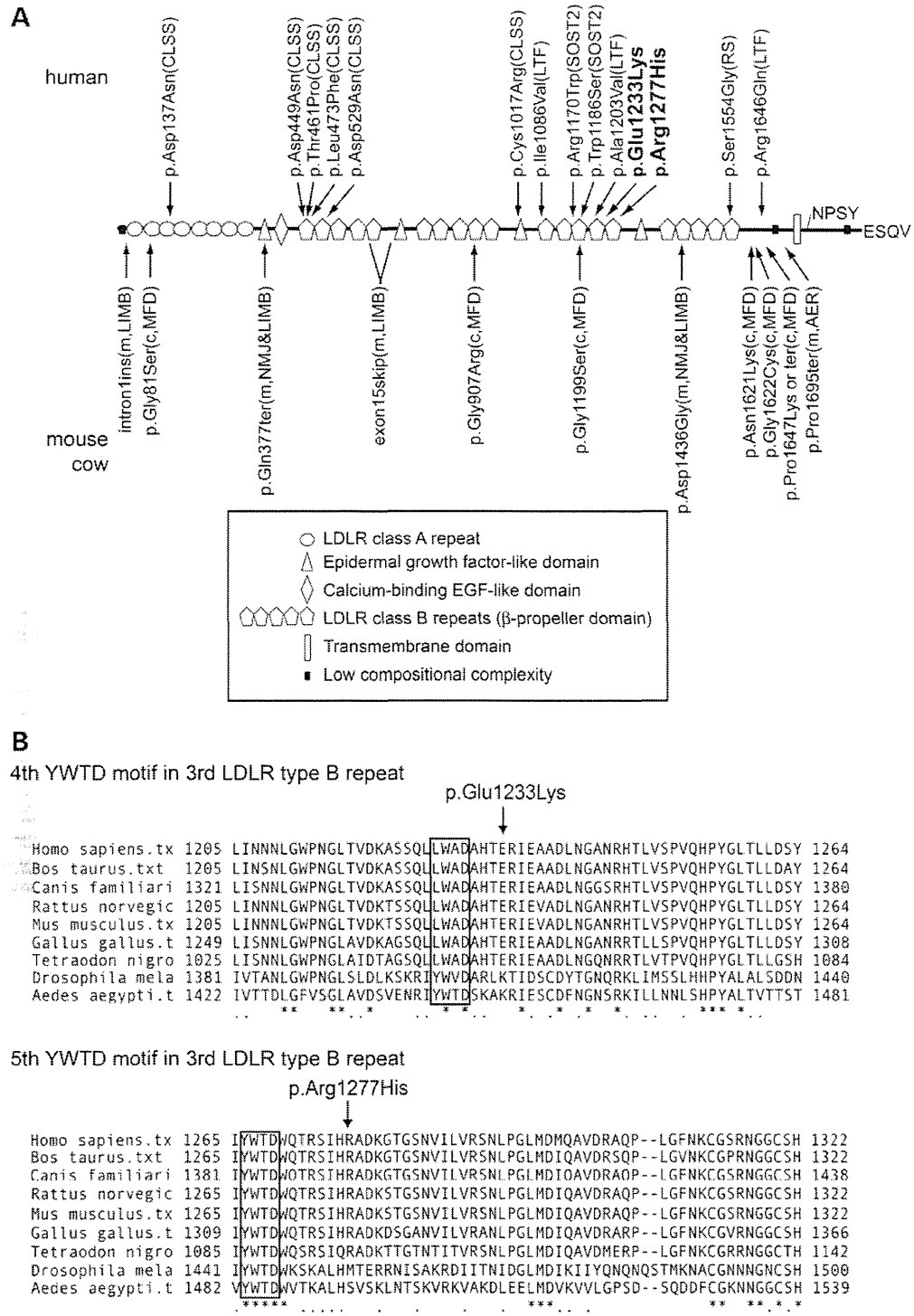

Figure 2. Structure and previously identified mutations of LRP4. (**A**) Domain structure of LRP4 and positions of reported mutations in human, mouse and cow. p.Glu1233Lys (EK mutation) and p.Arg1277His (RH mutation) in the current studies are shown in bold. In human, LRP4 mutations cause CLSS (MIM 212780) and sclerosteosis-2 (SOST2, MIM 614305). SNPs are also associated with an increased risk for Richter syndromes (RS) and a low-trauma fracture (LTF) due to decreased bone mineral density. In mouse, mutations cause abnormal development of the apical ectodermal ridge (AER) leading to polysyndactyly and tooth abnormality, as well as abnormal developments of limbs (LIMB) and the neuromuscular junctions (NMJ). In cow, mutations lead to mulefoot disease (MFD). LRP4 harbors eight low-density lipoprotein receptor (LDLR) domain class A, four epidermal growth factor-like domains, a calcium-binding EGF-like domain, four LDLR class B repeat (β-propeller domain), a transmembrane domain and an intracellular domain. The LDLR type B repeat contains five tandem repeats of an YWTD motif to build a propeller-like structure. NPSY close to the C-terminal end is a motif for endocytosis and ESQV at the C-terminal end is a motif for binding to PDZ-containing proteins. (**B**) Positions of the EK and RH mutations downstream of the 4th and 5th YWTD motifs (boxed). The amino acid sequences are highly conserved across vertebrates but not in insects. Asterisks indicate strictly conserved amino acids, and dots indicate loosely conserved amino acids.

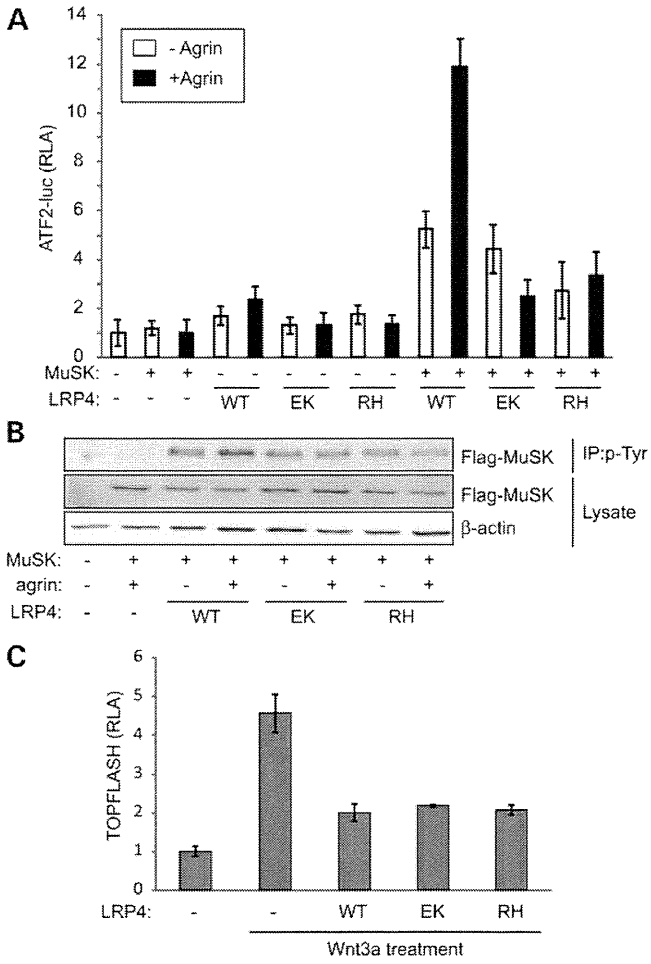

Figure 3. p.Glu1233Lys (EK) and p.Arg1277His (RH) mutants compromise agrin-mediated upregulation of MuSK signaling but retain Wnt-suppressive activity in HEK293 cells. (**A**) ATF2-luciferase reporter assay of HEK293 cells to quantify agrin-mediated activation of the MuSK signaling pathway. Cells were transfected with ATF2-luc reporter and Renilla reporter plasmids along with MuSK cDNA and the indicated LRP4 cDNA. Cells were cultured with or without 10 ng/μl agrin. Wild-type (WT) LRP4-activated MuSK without agrin, and agrin further enhanced the activation. The EK and RH mutations compromise MuSK activation in the presence or absence of agrin. (**B**) MuSK phosphorylation assay of HEK293 cells transfected with Flag-MuSK and the indicated *LRP4* cDNA with or without agrin (10 ng/μl). Phosphorylated MuSK was detected by immunoprecipitation of cell lysate by anti-phosphotyrosine antibody (p-Tyr) followed by immunoblotting with anti-FLAG antibody. Wild-type LRP4 phosphorylates MuSK, which is further enhanced by agrin, but EK and RH mutants abolish responsiveness to agrin. (**C**) TOPFLASH reporter assay of HEK293 cells to quantify responsiveness to Wnt3a. Cells were transfected with the TOPFLASH reporter and Renilla reporter plasmids along with the indicated *LRP4* cDNA. Cells were cultured in the presence or absence of Wnt3a. Means and SD are indicated. Wild-type (WT) and mutant LRP4 (EK and RH) suppress the Wnt3a-mediated signaling to the same extent.

expressed on the cell surface, beneath the cell membrane or secreted from the cells.

Mutations in *LRP4* causing sclerosteosis-2 have No effect on MuSK signaling

In contrast to our EK and RH mutations in the 3rd β-propeller domain, p.Arg1170Trp (abbreviated as RW) and p.Trp1186Ser (WS) mutations identified in a patient with sclerosteosis-2 impair Wnt-suppressing activity of LRP4 (12). We first confirmed that wild-type LRP4 and the two mutants are similarly expressed on the plasma membrane in HEK293 cells (Fig. 6A) as we observed in COS7 cells (Supplementary Material, Fig. S1). We then analyzed the effects of the two mutations on MuSK (Fig. 6B) and Wnt (Fig. 5C) signaling. Consistent with the previous report (12), the RW and WS mutations abrogated the Wnt-suppressing activity of LRP4 (Fig. 6C) but had no effect on agrin-induced MuSK signaling (Fig. 6B). Cell surface-binding assay also confirmed that the two mutants retained their ability to bind to agrin and MuSK (Fig. 6D).

As the four mutations affecting MuSK or Wnt signaling were all in the 3rd β-propeller domain, we scrutinized the positions of mutations by homology modeling of the 3rd β-propeller domain of human LRP4 using the 1st β-propeller domain of human LRP6 (PDB ID: 3SOV). The 3rd β-propeller domain contains six blade-like structures and displays a YWTD motif at the second β sheet below the surface of each blade (Fig. 7A and Supplementary Material, Movie S1). In this model, the EK and RH mutations, which only affect agrin/LRP4/MuSK signaling, are located on edge of the 5th and 6th blades, respectively (Fig. 7B and Supplementary Material, Movie S1). In contrast, the RW and WS mutations, which only affect Wnt signaling, are located in a central cavity of the propeller (Fig. 7C and Supplementary Material, Movie S1).

Artificially engineered Lrp4 mutations at the edge of the 3rd β-propeller domain affect MuSK signaling and those in the central cavity affect Wnt signaling

To further confirm that the edge of the 3rd β-propeller domain mediates MuSK signaling and that the central cavity mediates Wnt signaling, we introduced four other artificial mutations based on structural modeling of the 3rd β-propeller domain (Fig. 7A and Supplementary Material, Movie S1). As RH and EK mutations affected two exposed amino acids on the 2nd β sheet, we introduced an alanine into two neighboring amino acids to make IA and VA mutations (Fig. 7B and Supplementary Material, Movie S1). Similarly, as WS and RW mutations were facing the central cavity of the 3rd β-propeller domain, we introduced an alanine into the corresponding amino acids in the other blades to make YA and NA mutations (Fig. 7C and Supplementary Material, Movie S1). We then examined the effects of each mutation on MuSK and Wnt signaling. As expected, the VA and IA mutations at the edge of the 3rd β-propeller domain affected MuSK signaling (Fig. 8A), but not Wnt signaling (Fig. 8B). In contrast, the NA and YA mutations in the central cavity normally activated MuSK signaling (Fig. 8A), but lost Wnt-suppressive activity (Fig. 8B). Similarly, the cell surface-binding assay showed that the VA and IA mutations reduced binding of agrin and MuSK (Fig. 8C and D). Thus, the artificial mutations further underscore the differential signaling roles of the edge and the central cavity of the 3rd β-propeller domain.

DISCUSSION

LRP4 mutations cause a novel CMS

Because mutations in *AGRN* (25) and *MUSK* (26) have been known to cause CMS and because LRP4 was shown to be a

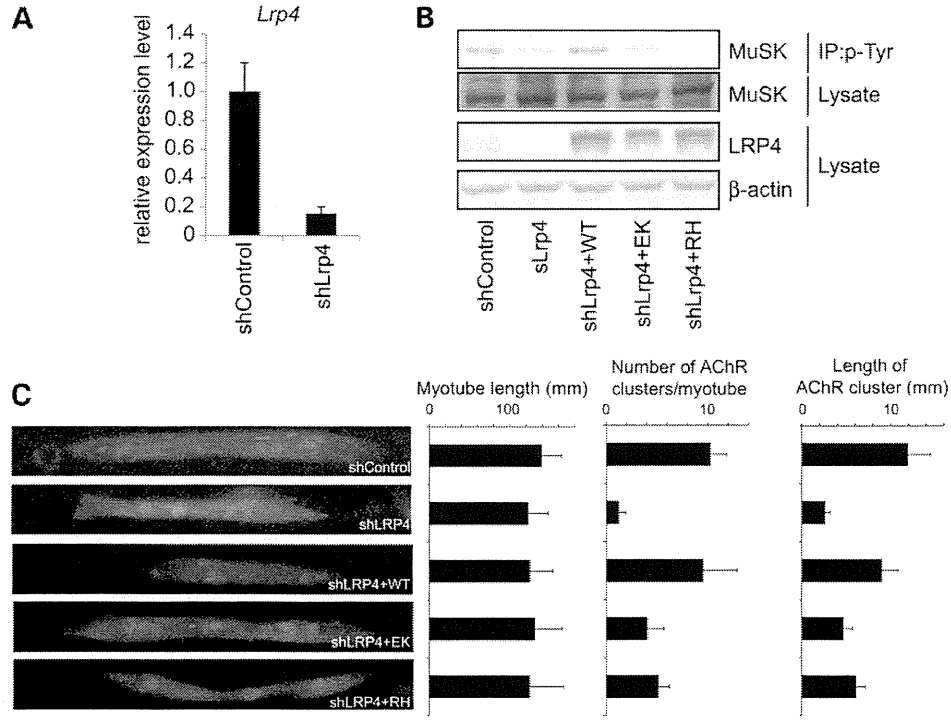

Figure 4. p.Glu1233Lys (EK) and p.Arg1277His (RH) mutants compromise agrin-mediated upregulation of MuSK signaling and AChR clustering in C2C12 myoblasts/myotubes. (**A**) Endogenous Lrp4 expression in C2C12 myoblasts is suppressed by shRNA against mouse Lrp4 (shLrp4) by qRT-PCR. (**B**) MuSK phosphorylation assay of differentiation-induced C2C12 myoblasts transfected with shControl or shLrp4 and the indicated *LRP4* cDNA. Phosphorylated MuSK was detected by immunoprecipitation of cell lysate by anti-phosphotyrosine antibody (p-Tyr) followed by immunoblotting with anti-MuSK antibody. Wild-type LRP4, but not EK and RH mutants, phosphorylates MuSK in Lrp4-deficient myoblasts. (**C**) Agrin-mediated AChR clustering in C2C12 myotubes. Myotubes are transfected with EGFP cDNA, shLRP4 and the indicated *LRP4* cDNA using electroporation. AChR is visualized with Alexa594-conjugated α-bungarotoxin at 12 h after adding 10 ng/ml agrin. Right panels: Morphometric analysis showing that wild-type (WT) LRP4, but not EK and RH mutants, rescues the number and the length of AChR clusters in Lrp4-downregulated C2C12 myotubes. LRP4 has no effect on myotube length.

coreceptor for agrin that mediates activation of MuSK (Fig. 7D) (2,3). *LRP4* has been a candidate gene for a CMS for a number of years. In this communication, we show that mutations in *LRP4* cause a CMS and that the identified mutations affect MuSK signaling by compromising binding of LRP4 to both agrin and MuSK.

Our data predict that the identified *LRP4* mutations interfere with agrin-LRP4-MusK signaling and thereby hinder concentration of AChR on the junctional folds as well as normal development and maintenance of the entire junction. Our EP studies show that the synaptic contacts are dysplastic (Fig. 1) and that the nerve terminal and postsynaptic areas at the EP regions are hypoplastic (Table 1), but the AChR content of EPs and the synaptic response to ACh are not appreciably reduced. Because the patient has a myasthenic disorders by clinical and EMG criteria, we attribute sparing of the intercostal muscles to different expressivity of the genetic defect in different muscles. Sparing of selected muscles can occur in both autoimmune and congenital myasthenias and is indicated by absence of muscle weakness or a decremental EMG response from some muscles in either disorder. For example, in MuSK antibody-positive myasthenia, EPs in intercostal and biceps brachii muscles have a normal AChR content, generate normal MEPP amplitudes, and have well preserved junctional folds (27,28). Analysis of *Musk* and *Lrp4* expressions in mouse muscles by quantitative RT–PCR revealed that expressions of *Musk* in omohyoid and trapezius muscles were less than those in the other muscles (Supplementary Material, Fig. S2). The least expression of *Musk* in mouse omohyoid has been recently reported (29). In contrast, *Musk* expression in intercostal muscle was ~three times more compared with omohyoid. Although human specimens of various muscles were not available for our studies, high and low MuSK expressions in intercostal and trapezius muscles may partly account for spared and impaired NMJ signal transmissions in intercostal and trapezius muscles, respectively, in our patient with *LRP4* mutations.

Position-specific disease phenotypes of *LRP4* mutations

The extracellular domain of LRP4 is known to bind to several proteins: agrin (2,3), MuSK (4), Wnt ligands (30), dkk1 (31), a Wnt inhibitor (32,33), sclerostin (31), another Wnt inhibitor (32,33) and possibly apoE (34). Specific binding domains of LRP4 have been dissected: agrin binds to the LDLa repeats 6–8, EGF-like domains, and the 1st β-propeller domain (Fig. 7B and Supplementary Material, Movie S1) (4,23); MuSK binds to the 4th/5th LDLa repeats and the 3rd β-propeller domain (4); sclerostin binds to the 3rd β-propeller domain (12); and apoE binds to LDLa (34). As for Wnt ligands, the precise molecular mechanisms how LRP4 suppresses Wnt signaling remain elusive, although the Wnt-suppressive effect of LRP4 is well established (35).

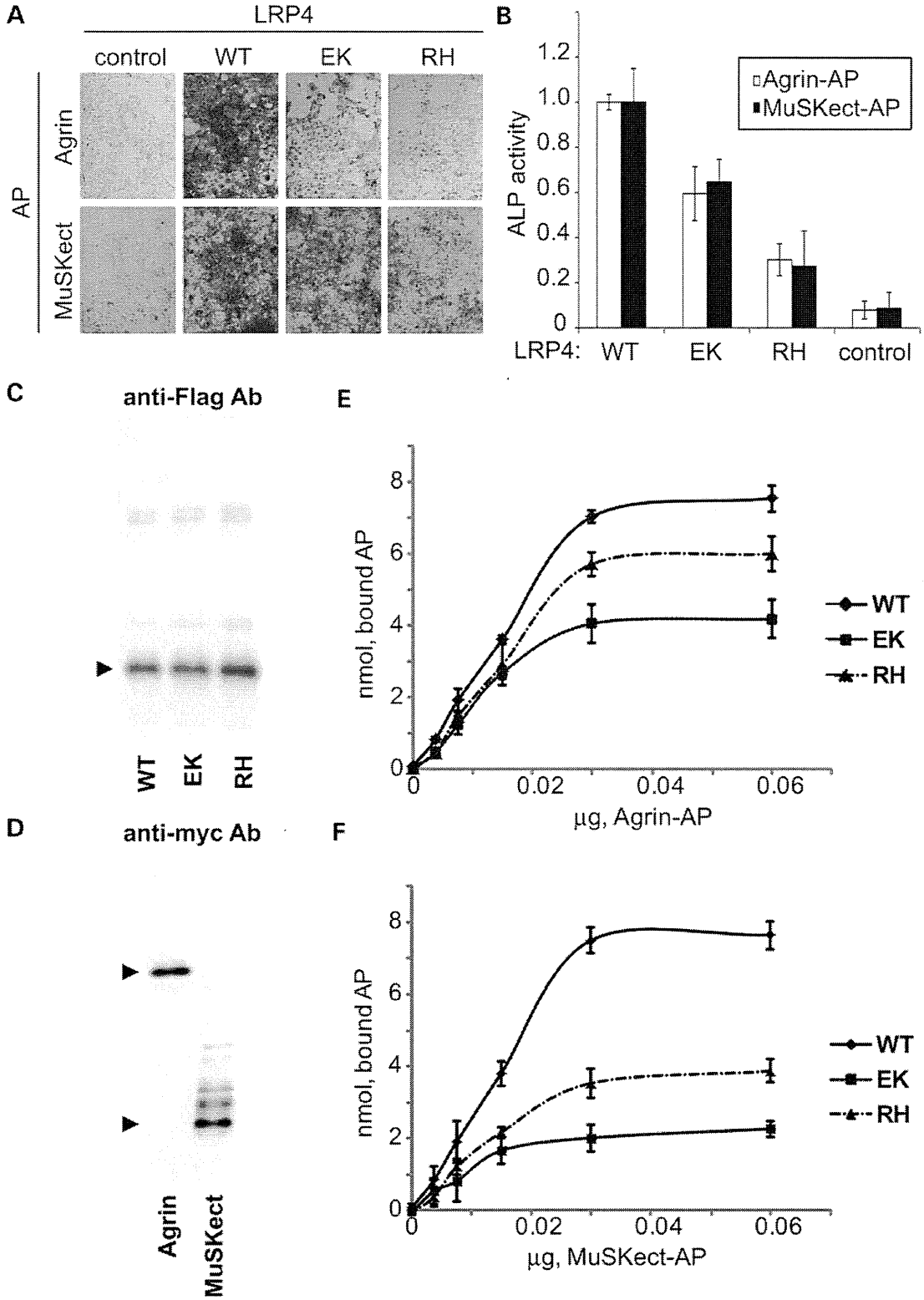

Figure 5. The p.Glu1233Lys (EK) and p.Arg1277His (RH) mutants impair binding of LRP4 to MuSK and agrin. (**A** and **B**) Cell surface-binding assays. COS7 cells were transfected with the wild-type or mutant *LRP4* cDNA and added with concentrated conditioned medium containing either neural Agrin-mycAP or MuSKect-mycAP as indicated. Control cells were transfected with an empty vector. Bound MuSKect-mycAP or agrin-mycAP was stained for the alkaline phosphatase activity (A). (B) The mean and SD of ALP activities of bound agrin-mycAP and MuSKect-mycAP in three independent wells. The RH and EK mutants reduce binding of MuSKect-mycAP and agrin-mycAP. (**C** and **D**) Western blotting with an anti-Flag antibody for detecting LRP4ecd-Flag; and anti-myc antibody for agrin-myc and MuSK-myc. All the transfected cDNAs were similarly expressed. (**E** and **F**) *In vitro* plate-binding assays. Plates were coated with the wild-type or mutant LRP4ecd-Flag protein and overlaid with purified agrin-mycAP protein (E) and MuSKect-mycAP (F). The EK and RH mutants reduce binding affinities for MuSKect-mycAP and agrin-mycAP. Mean and SE are plotted ($n = 4$; $P < 0.05$ for both MuSKect-mycAP and agrin-mycAP by two-way ANOVA).

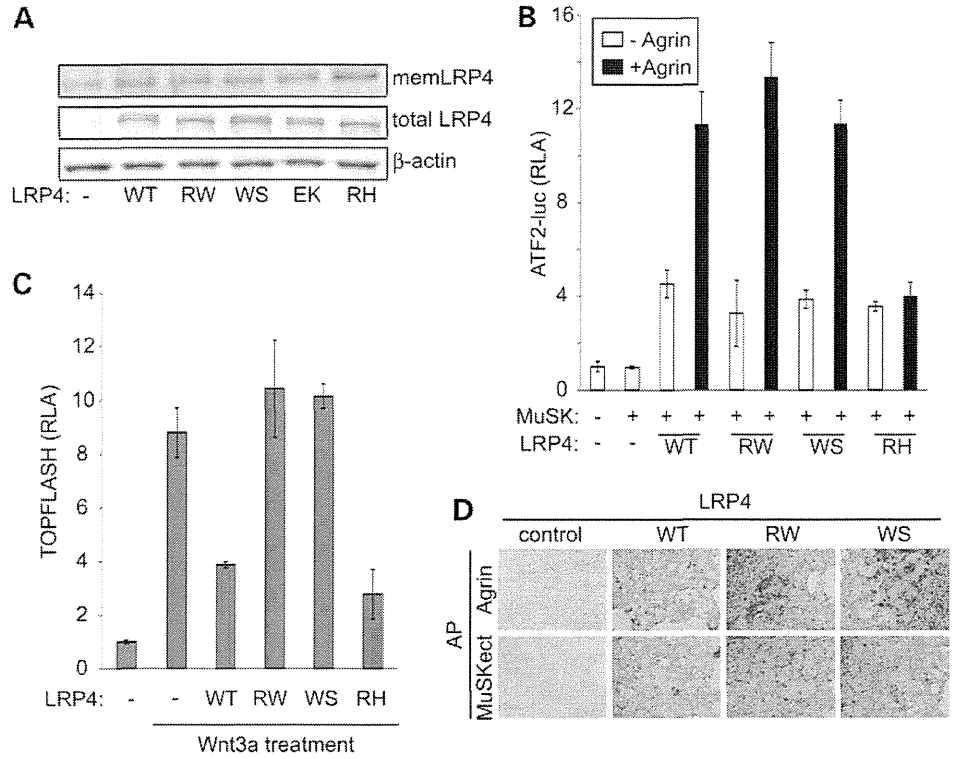

Figure 6. The p.Arg1170Trp (RW) and p.Trp1186Ser (WS) mutants retain the activity of agrin-mediated upregulation of MuSK signaling but compromise Wnt-suppressive activity. (**A**) Western blotting with an anti-Flag antibody for detecting full-length LRP4-Flag. Membrane proteins are biotinylated and precipitated with streptavidin. β-Actin proteins in each sample were detected as loading control. (**B** and **C**) ATF2-luciferase (B) and TPOFLASH (C) reporter assays of HEK293 cells to quantify activation of MuSK and Wnt signaling pathways, respectively. The RH mutant is included as a control. Means and SD of three independent experiments are indicated. (**D**) Cell surface-binding assays as in Figs 5A and B. Both the RW and WS mutants are able to bind to agrin-mycAP (upper) and MuSKect-mycAP (lower).

The diverse array of binding partners enables LRP4 to play an essential role in multiple biological processes including limb and kidney morphogenesis (16,31); bone development through cell fate decision and migration (35); and synaptogenesis (6,34). The multiple phenotypes caused by mutations in the 3rd β-propeller domain prompted us to scrutinize different regions of this domain, and we found that the edge mediates MuSK signaling and the central cavity mediates Wnt signaling. That a single missense mutation in the 3rd β-propeller domain compromises LRP4 binding to MuSK supports a previous observation that MuSK is bound to the 3rd β-propeller domain of LRP4 (Fig. 7B and Supplementary Material, Movie S1) (4). In contrast, reduced binding of our LRP4 mutants to agrin was unexpected because agrin binds to the EGF-like domain, LDLa repeats 6–8 and the 1st β-propeller domain (4,23). The 2nd and 3rd β-propeller domains, however, enhance binding to agrin to ~170% of the truncated LRP4 lacking these domains (4). Accordingly, mutations in the 3rd β-propeller domain in our patient are likely to compromise the enhancing effect conferred by the 3rd β-propeller domain of LRP4.

MATERIALS AND METHODS

Patient

All human studies were in accord with and approved by the Institutional Review Boards of the Mayo Clinic and Nagoya University Graduate School of Medicine. The patient's father gave informed consent for the patient to participate in the study. Venous blood sample was obtained from the patient and his father and genomic DNA was isolated with the QIAamp Blood DNA kit (Qiagen) according to the manufacturer's recommendations.

Neuromuscular junction studies

Intercostal muscle specimens were obtained from the patient and from control subjects without muscle disease undergoing thoracic surgery. Cryosections were used to colocalize the acetylcholine receptor (AChR) and acetylcholine esterase (AChE) as described (36). AChE was also visualized on teased, glutaraldehyde-fixed muscle fibers cytochemically (37). EPs were localized for electron microscopy (38) and quantitatively analyzed (39) by established methods. Peroxidase-labeled α-bgt was used for the ultrastructural localization of AChR (40). The number of AChRs per EP was measured with [^{125}I]α-bgt. The amplitude of the miniature EP potential (MEPP) and EP potential (EPP) amplitudes and estimates of the quantal content of the EPP (*m*) were measured as previously described (41,42). Single-channel patch-clamp recordings were performed as previously described (43,44).

Exome-capture resequencing analysis

We enriched exonic fragments using the SureSelect human all exon v2 (Agilent Technologies) and sequenced 50 bp of each